1
2
3
4
5
6
7
8
9
10
11
12
13
14
15
16
17
18
19
20
21
22
23
24
25
26
27
28
29
30
31
32
33
34
35
36
37
38
39
40
41
42
43
44
45
46
47
48
49
50
51
52
53
54
55
56
57
58
59
60

Joint Precoder, Reflection Coefficients, and Equalizer Design for IRS-Assisted MIMO Systems

Wen Zhou, Chunguo Li, Lisheng Fan, Junjuan Xia, and Arumugam Nallanathan,

Fellow, IEEE

Abstract

The incorporation of intelligent reflecting surface (IRS) into wireless communication systems can extend the coverage and enhance the data transmission rate. This paper studies the joint transceiver and IRS designs in IRS-assisted multi-input multi-output (MIMO) systems under both perfect channel state information (CSI) and imperfect CSI. Specifically, the transmit precoder, reflection coefficients at the IRS, and receive equalizer are jointly optimized to minimize the data detection mean square error (MSE), subject to the transmission power constraint and the modulus constraints for IRS reflection coefficients. The design problems, non-convex and challenging, are tackled under the framework of alternating optimization. For the design with perfect CSI, we successively optimize the IRS reflection coefficients given the precoder and present the closed-form optimal angle of one reflection coefficient given the others. For the robust design with imperfect CSI, we first average the detection MSE over channel uncertainties by using a generalized statistical CSI error model. Then, the averaged MSE is approximated by a more tractable upper bound. Subsequently, the robust design problem is elaborately transformed into a form similar to the problem with perfect CSI. Numerical results demonstrate the effectiveness of the proposed designs as compared to various benchmark schemes.

Index Terms

Intelligent reflecting surface (IRS), multi-input multi-output (MIMO), robust design, channel state information (CSI).

W. Zhou is with the Department of Electronic Engineering, Nanjing Forestry University, Nanjing, China.
C. Li is with the School of Information Science and Engineering, Southeast University, Nanjing, China.
L. Fan and J. Xia are with the School of Computer Science, Guangzhou University, Guangzhou, China.
A. Nallanathan is with the School of Electronic Engineering and Computer Science, Queen Mary University of London, London, U.K.

2

I. INTRODUCTION

The fifth-generation (5G) mobile communication is required not only to provide users with more immersive business experiences, but also solve the communication problem between people and things, things and things. This leads to the emergence of a few dominant candidates, such as massive multi-input multi-output (MIMO), milimeter wave (mmWave), carrier aggregation. Though the candidates can meet the requirements of 5G to some degree, there still exist some problems. The mmWave signal is easily blocked by buildings and vulnerable to bad weather. The hardware of massive MIMO is difficult to implement due to dedicated radio frequency chains. Besides, the increase of users and services will result in high energy consumption. All these bring about new challenges to 5G systems [1].

To alleviate the dilemma, the intelligent reflecting surface (IRS) has emerged. The IRS consists of a large array of passive scattering elements with low cost. By deploying it in the radio environment, e.g. advertising panels and building walls, the IRS can assist wireless communications and information sensing effectively. Hence, it attracts a lot of attention from the academia as well as the industry and various works have been conducted in the IRS-related area from hardware implementation [2] to algorithm design.

The existing studies showed that the joint transmitter and IRS design could improve the system performance [3]–[20]. Specifically, the communication rate or capacity optimization was conducted in [4]–[11]. For instance, the capacity of IRS-aided MIMO systems was enhanced by jointly optimizing the MIMO transmission covariance and the reflection coefficients at the IRS [6], [8], while a genetic algorithm (GA) was proposed to maximize the sum rate of all users in IRS-aided multiple-input single-output (MISO) systems [9]. Moreover, some researches considered the optimization of symbol error rate (SER) [12] and signal-to-noise-plus-interference ratio (SINR) [13] in IRS-aided systems. With discrete phase shifts, the IRS reflecting elements and the precoder at the transmitter were jointly optimized to minimize the SER for IRS-aided point-to-point MIMO systems [12]. A multi-beam multi-hop routing problem for a multi-IRS aided multiuser MISO system was studied in [13], where the optimal IRSs and their beam routing paths for users were selected and the beamforming at the BS/IRSs was designed in order to maximize the minimum received signal power among users. Aiming at minimizing the transmit power, the transmit precoding at the access point (AP) and the reflect phase shifts at

the IRS for IRS-aided MISO systems were jointly designed [16], [17]. In further, there were also a few works that minimized the detection mean square error (MSE) at the receiver so as to improve the IRS-aided system performance [19], [20]. For example, the problem of model aggregation for the federated learning with the aid of multiple IRSs was studied in [19], in which the transmit power at devices, the receive scalar at the base station, and the phase shifts at IRSs were jointly designed by minimizing the MSE. Currently, the IRS-aided MISO or single-input single-output (SISO) systems have been extensively studied [3], [4], [9], [13]–[19], while there is still research room for IRS-aided MIMO systems.

Note that the aforementioned literature [3]–[20] requires perfect channel state information (CSI). However, due to the limited length of pilot sequences and the feedback latency, perfect CSI is difficult to be obtained in practice. Taking the estimated CSI as perfect will cause the system performance degradation. Hence, the robust design against the CSI error in IRS-aided systems is of significance and a few related works have been conducted [21]–[29]. Aiming at minimizing the transmission power subject to some quality of service (QoS) constraints, the beamformer at the transmit and phase shifts at the IRS were jointly designed in [21]–[24]. For instance, a robust design framework was proposed for IRS-aided communication systems in the presence of user location uncertainty [24], where the transmit beamformer and IRS phase shifts were designed in order to minimize the transmit power while ensuring the user rate is above a threshold for all possible user location error realizations. The robust transmission designs for IRS-aided multi-antenna systems in the presence of channel uncertainties have been proposed to maximize the system sum rate [25], [26]. Besides, some researches considered the problem about the detection MSE [27] or energy efficiency [29]. However, most current works focused on the IRS-aided MISO system [22]–[29]. To the best of our knowledge, there have been no works on the robust design for IRS-aided MIMO systems.

From the above literature review, we can see that there is still much room for the study of IRS-aided MIMO systems. Compared with MISO systems in which only a single beamformer is considered, multiple beamformers that form the precoder matrix should be designed at the transmitter of the IRS-aided MIMO system. The IRS reflection coefficients need to enhance the effective channel composed of a direct link and a few cascaded channels, meanwhile balancing the power allocation among multiple beamformers. Moreover, the coupling between the precoder matrix and the IRS reflection coefficients becomes more complicated. Mathematically, the objects

handled by the problem in IRS-aided MIMO systems are matrices whose processing is usually more difficult than vectors in MISO systems. Next, we discuss the criterion of the joint design in this article. A few performance metrics can be considered as the design criteria, e.g., the capacity [6], [8], SER [12], outage, and MSE. Usually, the capacity is derived with the assumptions of Gaussian codes used by the transmitter and Gaussian noises in the channel [30], whereas the MSE has no such assumptions, the optimization of which has more applications, e.g. the case of non-Gaussian noise. On the other front, compared with the SER-based metric, optimizing MSE is more likely to obtain the solution analytically. Due to these reasons, we adopt the MSE-based metric for the design. The main difficulties for the joint design in IRS-aided MIMO systems lie in that the coupling between the precoder and IRS reflection coefficients and the inverse of a matrix parameterized by many variables. Moreover, the coupling is more complicated for the case of imperfect CSI by comparing with the perfect-CSI case, which brings more challenges to the joint design.

Based on the above, with the MSE-based metric, this paper studies the joint transceiver and IRS design for IRS-aided MIMO systems under both the perfect CSI and imperfect CSI. Specifically, the precoder at the transmitter, reflection coefficients at the IRS, and equalizer at the receiver are jointly optimized in order to minimize the data detection MSE. The main contributions of this work are outlined as follows:

1) To the best of our knowledge, this is the first work to study the joint transceiver and IRS design whose aim is to minimize the data detection MSE. This is also the first work to study the robust joint transceiver and IRS design against channel uncertainties for IRS-assisted MIMO systems, whereas the most previous robust designs are for MISO systems[1].

2) For IRS-aided MIMO systems with perfect CSI, we formulate the joint design problem that minimized the detection MSE subject to the transmission power constraint and the modulus constraints for IRS reflection coefficients. The problem, nonconvex and hence challenging, is solved under the framework of alternating optimization. Given the precoder, we exploit

---

[1]The main differences between this paper and [27] lie in two aspects: 1) The system models are different, i.e., the MIMO system is used in this paper instead of the MISO system in [27]; 2) the channel error models are also different, i.e., the error model of this paper considers the channel correlation while [27] did not consider it. In addtion, there are two major differences between this paper and [20]. One difference is that [20] adopts the nonlinear transceiver, i.e., Tomlinson-Harashima precoding at the transmitter and decision feedback equalizer at the receiver, while this paper uses a linear structure. Another difference is that we consider the optimization for the amplitudes of IRS reflecting coefficients, instead of the unit-modulus assumption in [20].

an iterative algorithm and solve the reflection coefficients successively, i.e., each time only one coefficient is optimized. The optimal angle of the coefficient is derived in a closed form while the optimal modulus can be found via one-dimension (1D) line search.

3) For IRS-aided MIMO systems with imperfect CSI, we present a more generalized statistical CSI error model in which only the first and second moments are specified while the distribution is not. With this model, we average the detection MSE over CSI errors and formulate the robust design problem that minimizes the average MSE subject to two constraints. Since the objective of the problem is intractable, we derive an upper bound and replace the original objective. After a few elaborate manipulations, the robust design problem is arranged into a form similar to the problem with perfect CSI, and hence can be readily solved.

4) The joint transceiver and IRS designs under both perfect CSI and imperfect CSI are evaluated by extensive numerical results. The results show that, the proposed joint design under perfect CSI is able to achieve the lowest detection MSE among all the benchmark schemes. Compared with the non-robust design, the proposed robust design against channel uncertainties exhibits significantly better performance in terms of both MSE and bit error rate (BER). Even with imperfect CSI, the exploitation of IRS has benefits to the improvement of system performance.

The rest of this paper is organized as follows. The IRS-aided MIMO system model is described in Section II. The joint transceiver and IRS design with perfect CSI is considered in Section III, while the robust joint design against the imperfect CSI is studied in Section IV. The effects of various system parameters on the performance of the proposed algorithms are presented in Section V, followed by conclusions in Section VI.

Notations: Vectors are denoted by boldface lowercase letters and matrices are denoted by boldface uppercase letters. $\mathbb{C}^{m \times n}$ represents the set of $m \times n$ complex matrices. For a scalar x, $\lfloor x \rfloor$ takes its integer part. For a vector $\mathbf{x}$, $\text{diag}\{\mathbf{x}\}$ stands for a square diagonal matrix with $\mathbf{x}$'s elements on the main diagonal; $\mathbf{x} \succeq \mathbf{0}$ means $x_i \geq 0, \forall i$, where x_i is the i-th entry of $\mathbf{x}$. For a matrix $\mathbf{X}$, the notations $\mathbf{X}^*$, $\mathbf{X}^T$, and $\mathbf{X}^H$ denote the conjugate, transpose, and Hermitian transpose of $\mathbf{X}$, respectively; $\text{Tr}(\mathbf{X})$ and $\text{rank}(\mathbf{X})$ denote the trace and rank of $\mathbf{X}$, respectively; $\text{Re}(\mathbf{X})$ and $\text{Im}(\mathbf{X})$ take the real and imaginary part of $\mathbf{X}$, respectively; $[\mathbf{X}]_{m,n}$ is the (m, n)-th entry of $\mathbf{X}$; $\mathbf{X} \succeq \mathbf{0}$ means that $\mathbf{X}$ is positive semidefinite. We write $\mathcal{CN}(\boldsymbol{\mu}, \mathbf{R})$ to represent a
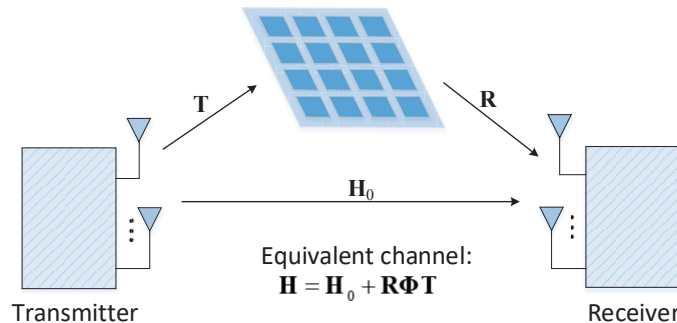
Fig. 1: The system diagram.

complex Gaussian distribution with mean $\boldsymbol{\mu}$ and covariance matrix $\mathbf{R}$. Besides, $\|\cdot\|_F$ denotes the Frobenius norm, $\mathbb{E}(\cdot)$ denotes the statistical expectation, and $\mathbf{I}_m$ is an $m \times m$ identity matrix.

II. SYSTEM MODEL

As in Fig. 1, consider an IRS-assisted MIMO communication system with N_T transmit antennas and N_R receive antenna. The incorporation of the IRS provides a non-light-of-sight (NLOS) path between the transmitter and the receiver and hence improves the communication quality. The IRS consists of M independent reflection elements whose coefficients can be dynamically adjusted by a controller. The coefficient of the m-th element is expressed by $\alpha_m = \rho_m e^{j\theta_m}$, where $0 \leq \rho_m \leq 1$ and $0 \leq \theta_m < 2\pi$ are the amplitude and phase of element m. The transmitted signal arrives at the receiver through both the direct and reflection paths. Denote by $\mathbf{H}_0 \in \mathbb{C}^{N_R \times N_T}$, $\mathbf{R} \in \mathbb{C}^{N_R \times M}$, and $\mathbf{T} \in \mathbb{C}^{M \times N_T}$ the channel matrices from the transmitter to receiver, the IRS to receiver, and the transmitter to IRS, respectively. The equivalent channel matrix between the transmitter and receiver is given by [6]

$$
\begin{aligned}
\mathbf{H} &= \mathbf{H}_0 + \mathbf{R}\boldsymbol{\Phi}\mathbf{T} \\
&= \sqrt{g_0}\boldsymbol{\Psi}_{R,0}^{\frac{1}{2}}\mathbf{H}_{w,0}\boldsymbol{\Psi}_{T,0}^{\frac{1}{2}} + \sqrt{g_2}\boldsymbol{\Psi}_{R,2}^{\frac{1}{2}}\mathbf{H}_{w,2}\boldsymbol{\Psi}_{T,2}^{\frac{1}{2}} \cdot \boldsymbol{\Phi} \cdot \sqrt{g_1}\boldsymbol{\Psi}_{R,1}^{\frac{1}{2}}\mathbf{H}_{w,1}\boldsymbol{\Psi}_{T,1}^{\frac{1}{2}},
\end{aligned}
\tag{1}
$$

where $\mathbf{R} \triangleq \sqrt{g_2}\boldsymbol{\Psi}_{R,2}^{\frac{1}{2}}\mathbf{H}_{w,2}\boldsymbol{\Psi}_{T,2}^{\frac{1}{2}}$ and $\mathbf{T} \triangleq \sqrt{g_1}\boldsymbol{\Psi}_{R,1}^{\frac{1}{2}}\mathbf{H}_{w,1}\boldsymbol{\Psi}_{T,1}^{\frac{1}{2}}$; g_0, g_1, and g_2 are the path losses of the direct link, the transmitter to IRS link, and the IRS to receiver link, respectively; $\boldsymbol{\Phi}$ is the reflection matrix and $\boldsymbol{\Phi} \overset{\Delta}{=} \mathrm{diag}\{\alpha_1, \cdots, \alpha_M\}$; $\mathbf{H}_{w,0} \in \mathbb{C}^{N_R \times N_T}$ consists of *i.i.d* complex Gaussian random variables with zero mean and unit variance, and $\mathbf{H}_{w,1} \in \mathbb{C}^{N_R \times M}$ and $\mathbf{H}_{w,2} \in \mathbb{C}^{M \times N_T}$ have similar definitions; $\boldsymbol{\Psi}_{R,0}$ and $\boldsymbol{\Psi}_{T,0}$ are the transmit and receive correlation matrices for the direct link, respectively; similarly, $\{\boldsymbol{\Psi}_{R,1}, \boldsymbol{\Psi}_{T,1}\}$ and $\{\boldsymbol{\Psi}_{R,2}, \boldsymbol{\Psi}_{T,2}\}$ are defined for the transmitter to IRS and the IRS to receiver links, respectively. Note that, the direct link, the

transmitter to IRS link, and the IRS to receiver link are numbered 0, 1, and 2, respectively.

Denote by $\mathbf{s} \in \mathbb{C}^{d \times 1}$ the data to be sent, where $1 \leq d \leq N_T$ is the number of symbols. With the aid of a linear precoder matrix $\mathbf{F} \in \mathbb{C}^{N_T \times d}$, the transmitted vector is expressed by $\tilde{\mathbf{s}} = \mathbf{F}\mathbf{s}$. We assume that the symbols of $\mathbf{s}$ are independent and with unit power, i.e., $\mathbb{E}\left(\mathbf{s}\mathbf{s}^H\right) = \mathbf{I}_d$. Hence, the average transmission power is $\mathbb{E}\left(\tilde{\mathbf{s}}^H\tilde{\mathbf{s}}\right) = \text{Tr}\left(\mathbf{F}\mathbf{F}^H\right)$, satisfying $\text{Tr}\left(\mathbf{F}\mathbf{F}^H\right) \leq P_T$, where P_T is the maximum transmission power. The received signal, denoted as $\mathbf{r} \in \mathbb{C}^{N_R \times 1}$, can be expressed as

$$\mathbf{r} = \mathbf{H}\mathbf{F}\mathbf{s} + \mathbf{n}, \tag{2}$$

where $\mathbf{n}$ is a zero-mean random vector with covariance $\mathbf{R_n}$.

At the receiver, with the aid of a linear equalization matrix $\mathbf{G} \in \mathbb{C}^{N_T \times N_R}$, the transmitted data is estimated by $\hat{\mathbf{s}} = \mathbf{G}\mathbf{r}$. Consequently, the MSE of data detection is given by

$$\text{MSE} = \mathbb{E}\left[(\hat{\mathbf{s}} - \mathbf{s})^H (\hat{\mathbf{s}} - \mathbf{s})\right] = \mathbb{E}\left\{\text{Tr}\left[(\mathbf{G}\mathbf{r} - \mathbf{s})(\mathbf{G}\mathbf{r} - \mathbf{s})^H\right]\right\}. \tag{3}$$

Notice that the transmitted data $\mathbf{s}$ has been normalized and hence, the MSE is normalized accordingly.

This paper aims at jointly designing $\mathbf{F}$, $\mathbf{G}$, and $\mathbf{\Phi}$ in order to minimize the detection MSE. In what follows, we will consider two cases according to whether perfect CSI is available for the system and design $\{\mathbf{F}, \mathbf{G}, \mathbf{\Phi}\}$ for them respectively.

Remark 1: On the system model, a few things need to be further discussed. First, the noise $\mathbf{n}$ is not limited to the Gaussian noise and it can be non-Gaussian and colored. Second, the transmit signal $\mathbf{x}$ can be either the Gaussian code or with simple signal constellations, e.g. BPSK. Third, the phase shifts of IRS reflection coefficients are assumed continuous instead of discrete. The proposed design in this paper is not suitable for the discrete case [16], in which the integer programming will be involved. Fourth, different from most literature, the amplitudes of IRS reflection coefficients in this paper are assumed to vary within $[0, 1]$. This may result in a complicated control. However, the corresponding research is still theoretically meaningful.

Remark 2: As in (1), the Kronecker model is used for the modelling of the equivalent channel. In fact, it has been widely used in current works [31], [32]. Ref. [31] discussed this model in detail and presented its suitability condition [31, Propositions 3.1, 3.2]. Besides, in general, there are three types of spatial correlation models for MIMO channels, including the physical parameter-based model [32]–[34], exponential type [35], and uniform type [36]. All these types

8

can be used for the IRS-assisted MIMO system model. The first type, though quite complicated, is an accurate model for real-world scenarios. Hence, it is used for most cases in the simulation. The second, a single-parameter model, is simple but allows one to study the correlation effect in an explicit way. Hence, for few cases where the effect of channel correlation is specially studied, the second type is used.

III. JOINT PRECODER, REFLECTION COEFFICIENTS, AND EQUALIZER DESIGN WITH PERFECT CSI

This section considers the case in which the system has perfect CSI. The joint precoder, reflection coefficients, and equalizer design is formulated as a nonconvex optimization problem. The alternating optimization framework is used to tackle this problem, where the problem is divided into two subproblems and the variables $\boldsymbol{\Phi}$ and $\mathbf{F}$ are optimized alternately. For the subproblem of optimizing $\boldsymbol{\Phi}$, the IRS reflection coefficients are successively optimized, i.e., each time only one single variable in $\{\alpha_m\}_{m=1}^M$ is optimized while the other $M-1$ variables are fixed. By doing so, the complicated coupling among these coefficients can be avoided.

To start with, the MSE in (3) is further expressed as

$$
\begin{aligned}
\text{MSE} &= \mathbb{E}_{\mathbf{n,s}} \left\{ \text{Tr} \left[(\mathbf{GHFs} + \mathbf{Gn} - \mathbf{s}) (\mathbf{GHFs} + \mathbf{Gn} - \mathbf{s})^H \right] \right\} \\
&= \text{Tr} \left\{ (\mathbf{GHF} - \mathbf{I}_d) \mathbb{E}_{\mathbf{s}} \left(\mathbf{ss}^H \right) (\mathbf{GHF} - \mathbf{I}_d)^H \right\} + \text{Tr} \left[\mathbf{G} \mathbb{E}_{\mathbf{n}} \left(\mathbf{nn}^H \right) \mathbf{G}^H \right] \qquad (4)\\
&= \text{Tr} \left[(\mathbf{GHF} - \mathbf{I}_d) (\mathbf{GHF} - \mathbf{I}_d)^H \right] + \text{Tr} \left[\mathbf{GR_n G}^H \right],
\end{aligned}
$$

where $\mathbf{R_n}$ is the covariance matrix of the noise vector $\mathbf{n}$. Given $\mathbf{F}$ and $\mathbf{H}$, the optimum linear receiver $\mathbf{G}^{\text{OPT}}$ is obtained by setting $\frac{\partial \text{MSE}}{\partial \mathbf{G}^*} = (\mathbf{GHF} - \mathbf{I}_d)(\mathbf{HF})^H + \mathbf{GR_n} = \mathbf{0}$, which yields

$$
\mathbf{G}^{\text{OPT}} = (\mathbf{HF})^H \left[\mathbf{R_n} + \mathbf{HF}(\mathbf{HF})^H \right]^{-1}. \qquad (5)
$$

Substituting $\mathbf{G}^{\text{OPT}}$ into (4), we have [37, Section IV.A]

$$
\begin{aligned}
\text{MSE} &= \text{Tr} \left[\mathbf{I}_d - (\mathbf{HF})^H \left(\mathbf{HFF}^H \mathbf{H}^H + \mathbf{R_n} \right)^{-1} \mathbf{HF} \right] \\
&= \text{Tr} \left[\left(\mathbf{I}_d + \mathbf{F}^H \mathbf{H}^H \mathbf{R_n}^{-1} \mathbf{HF} \right)^{-1} \right]
\end{aligned}. \qquad (6)
$$

With (6), the design problem is formulated as P_1. Note that, to highlight the two parameters $\mathbf{F}$ and $\boldsymbol{\Phi}$, we write the objective function as $\text{MSE}(\mathbf{F}, \boldsymbol{\Phi})$. It is clear that P_1 is nonconvex due to

the coupling of $\mathbf{F}$ and $\mathbf{\Phi}$. Hence, the alternating optimization framework is adopted so that the variables $\mathbf{F}$ and $\mathbf{\Phi}$ can be treated separately.

$$\mathrm{P}_1 : \min_{\mathbf{F},\mathbf{\Phi}} \mathrm{MSE}(\mathbf{F},\mathbf{\Phi}) = \mathrm{Tr}\left[\left(\mathbf{I}_d + \mathbf{F}^H\mathbf{H}^H\mathbf{R_n}^{-1}\mathbf{H}\mathbf{F}\right)^{-1}\right]$$

$$s.t.\ C_1 : \mathrm{Tr}\left(\mathbf{F}\mathbf{F}^H\right) \leq P_T$$

$$C_2 : |\alpha_m| \leq 1, m = 1\cdots M$$

$$C_3 : \mathbf{\Phi} = \mathrm{diag}\left\{\alpha_1, \cdots, \alpha_M\right\}.$$

A. The Framework of Alternating Optimization

Under the alternating optimization (AO) framework, we divide P_1 into two subproblems and solve them alternately.

1) Optimizing $\mathbf{F}$ given $\mathbf{\Phi}$: Clearly, given $\mathbf{\Phi}$, P_1 is convex with respect to $\mathbf{F}$. The optimal $\mathbf{F}$ has the following structure [37, Theorem 1]:

$$\mathbf{F} = \mathbf{U_F}\mathbf{\Lambda_F}, \tag{7}$$

where $\mathbf{U_F} \in \mathbb{C}^{N_T \times d'}$ has as columns the eigenvectors of $\mathbf{H}^H\mathbf{R_n}^{-1}\mathbf{H}$ corresponding to d' largest eigenvalues, $d' \triangleq \min\left(d, \mathrm{rank}\left(\mathbf{H_R}\right)\right)$, and $\mathbf{H_R} \triangleq \mathbf{H}^H\mathbf{R_n}^{-1}\mathbf{H}$; $\mathbf{\Lambda_F} = \left[\ \mathrm{diag}\left(\{\lambda_{\mathbf{F},i}\}_{i=1}^{d'}\right)\ \mathbf{0}\ \right] \in$ $\mathbb{C}^{d' \times d}$ with $\lambda_{\mathbf{F},i} = \sqrt{\left(\mu^{-\frac{1}{2}}\lambda_{\mathbf{H_R},i}^{-\frac{1}{2}} - \lambda_{\mathbf{H_R},i}^{-1}\right)^+}$, $\lambda_{\mathbf{H_R},i}$'s are the d' largest eigenvalues of $\mathbf{H_R}$, $(x)^+$ means $\max(x,0)$, and $\mu > 0$ satisfies the equation $\sum_{i=1}^{d'} \lambda_{\mathbf{F},i}^2 = P_T$.

2) Optimizing $\mathbf{\Phi}$ given $\mathbf{F}$: First, this subproblem, termed as P_2, is expressed as

$$\mathrm{P}_2 : \min_{\mathbf{\Phi}} \mathrm{MSE}(\mathbf{F},\mathbf{\Phi}) = \mathrm{Tr}\left[\left(\mathbf{I}_d + \mathbf{F}^H\mathbf{H}^H\mathbf{R_n}^{-1}\mathbf{H}\mathbf{F}\right)^{-1}\right]$$

$$s.t.\ C_2, C_3$$

For P_2, we would like to solve it by optimizing α_m's successively, i.e., each time only one variable α_m is optimized while α_i's with $i \neq m$ are fixed. The details are presented in the following subsection.

B. Successive Optimization of the Reflection Coefficients (SORC)

In this subsection, we propose an algorithm for optimizing the reflection coefficients $\{\alpha_m\}$ successively. That is, at each iteration, only one reflection coefficient α_m is optimized with $\{\alpha_i, i \neq m\}_{i=1}^M$ given.

To start with, we rewrite the effective channel $\mathbf{H}$ as

$$\mathbf{H} = \mathbf{H}_0 + \mathbf{R}\mathbf{\Phi}\mathbf{T} = \mathbf{H}_0 + \sum_{m=1}^{M} \alpha_m \mathbf{r}_m \mathbf{t}_m^T, \tag{8}$$

where $\mathbf{r}_m$ and $\mathbf{t}_m$ are the m-th columns of $\mathbf{R}$ and $\mathbf{T}^T$, respectively. Let $\tilde{\mathbf{H}}_0 = \mathbf{R}_\mathbf{n}^{-\frac{1}{2}}\mathbf{H}_0\mathbf{F}$, $\tilde{\mathbf{R}} = \mathbf{R}_\mathbf{n}^{-\frac{1}{2}}\mathbf{R}$, $\tilde{\mathbf{T}} = \mathbf{T}\mathbf{F}$, and $\tilde{\mathbf{H}} = \tilde{\mathbf{H}}_0 + \tilde{\mathbf{R}}\mathbf{\Phi}\tilde{\mathbf{T}}$. With (8), the MSE expression can be re-arranged as

$$\mathrm{MSE}(\mathbf{F}, \mathbf{\Phi}) = \mathrm{Tr}\left[\left(\mathbf{A}_m + \alpha_m\mathbf{B}_m + \alpha_m^*\mathbf{B}_m^H\right)^{-1}\right],$$

where $\mathbf{A}_m = \mathbf{I}_d + \left(\tilde{\mathbf{H}}_0 + \sum_{i=1,i\neq m}^{M} \alpha_i\tilde{\mathbf{r}}_i\tilde{\mathbf{t}}_i^T\right)^H \left(\tilde{\mathbf{H}}_0 + \sum_{i=1,i\neq m}^{M} \alpha_i\tilde{\mathbf{r}}_i\tilde{\mathbf{t}}_i^T\right) + |\alpha_m|^2\left(\tilde{\mathbf{r}}_m\tilde{\mathbf{t}}_m^T\right)^H\left(\tilde{\mathbf{r}}_m\tilde{\mathbf{t}}_m^T\right)$

and $\mathbf{B}_m = \left(\tilde{\mathbf{H}}_0 + \sum_{i=1,i\neq m}^{M} \alpha_i\tilde{\mathbf{r}}_i\tilde{\mathbf{t}}_i^T\right)^H \tilde{\mathbf{r}}_m\tilde{\mathbf{t}}_m^T$.

Then, given $\{\alpha_i, i \neq m\}_{i=1}^{M}$, we consider the following problem.

$$\mathrm{P}_{\text{2-m}}: \min_{\alpha_m} \mathrm{Tr}\left[\left(\mathbf{A}_m + \alpha_m\mathbf{B}_m + \alpha_m^*\mathbf{B}_m^H\right)^{-1}\right]$$

$$s.t. \ |\alpha_m| \leq 1$$

The module and phase of α_m will be treated separately. With $\alpha_m \triangleq \rho_m e^{j\phi_m}$, P2-m can be equivalently written as $\mathrm{P}_{\text{2-m}}: \min_{0\leq\rho_m\leq 1} f_1\left(\rho_m\right),$ where

$$f_1\left(\rho_m\right) = \min_{\phi_m} q(\rho_m, \phi_m) \triangleq \mathrm{Tr}\left[\left(\mathbf{A}_m + \rho_m e^{j\phi_m}\mathbf{B}_m + \rho_m e^{-j\phi_m}\mathbf{B}_m^H\right)^{-1}\right]. \tag{9}$$

Note that, for ease of exposition, we rewrite the MSE expression and define $q(\rho_m, \phi_m)$ with respect to ρ_m and ϕ_m in (9).

Given ρ_m, solving $f_1\left(\rho_m\right)$ can be divided into the following two cases according to whether $\mathrm{Tr}\left(\mathbf{A}_m^{-1}\mathbf{B}_m\right) = 0$.

1) $\mathrm{Tr}\left(\mathbf{A}_m^{-1}\mathbf{B}_m\right) \neq 0$: With the definition of $\mathbf{B}_m$, one has $\mathrm{rank}(\mathbf{B}_m) \leq 1$, leading to $\mathrm{rank}(\mathbf{A}_m^{-1}\times \mathbf{B}_m) \leq 1$. As $\mathrm{Tr}\left(\mathbf{A}_m^{-1}\mathbf{B}_m\right) \neq 0$, we must have $\mathrm{rank}(\mathbf{A}_m^{-1}\mathbf{B}_m) = 1$. Otherwise, $\mathrm{rank}(\mathbf{A}_m^{-1}\mathbf{B}_m) = 0$ will result in $\mathbf{A}_m^{-1}\mathbf{B}_m = \mathbf{0}$ and $\mathrm{Tr}\left(\mathbf{A}_m^{-1}\mathbf{B}_m\right) = 0$, which contradicts the prerequisite.

The function $q(\rho_m, \phi_m)$ can be further expressed as

$$q(\rho_m, \phi_m) = \mathrm{Tr}\left[\mathbf{A}_m^{-\frac{1}{2}}\left(\mathbf{I}_d + \rho_m e^{j\phi_m}\mathbf{A}_m^{-\frac{1}{2}}\mathbf{B}_m\mathbf{A}_m^{-\frac{1}{2}} + \rho_m e^{-j\phi_m}\mathbf{A}_m^{-\frac{1}{2}}\mathbf{B}_m^H\mathbf{A}_m^{-\frac{1}{2}}\right)^{-1}\mathbf{A}_m^{-\frac{1}{2}}\right]. \tag{10}$$

According to the Schur's triangularization theorem, any square complex matrix $\mathbf{X}$ is unitarily similar to a upper triangular matrix whose diagonal entries are $\mathbf{X}$'s eigenvalues [38, Theorem 2.3.1]. Therefore, $\mathbf{A}_m^{-\frac{1}{2}}\mathbf{B}_m\mathbf{A}_m^{-\frac{1}{2}}$ can be factorized as

$$\mathbf{A}_m^{-\frac{1}{2}} \mathbf{B}_m \mathbf{A}_m^{-\frac{1}{2}} = \mathbf{U}_m \mathbf{C}_m \mathbf{U}_m^H, \tag{11}$$

where $\mathbf{U}_m \in \mathbb{C}^{d \times d}$ is unitary, and $\mathbf{C}_m = (c_{ij})$ is upper triangular with diagonal entries $c_{11} \neq 0$ and $c_{ii} = 0, i \geq 2$. Clearly, $\mathrm{rank}(\mathbf{A}_m^{-1}\mathbf{B}_m) = 1$ is equivalent to $\mathrm{rank}(\mathbf{A}_m^{-\frac{1}{2}}\mathbf{B}_m\mathbf{A}_m^{-\frac{1}{2}}) = 1$; c_{11} is the unique nonzero eigenvalue of $\mathbf{A}_m^{-\frac{1}{2}}\mathbf{B}_m\mathbf{A}_m^{-\frac{1}{2}}$ and $c_{11} = \mathrm{Tr}\left(\mathbf{A}_m^{-\frac{1}{2}}\mathbf{B}_m\mathbf{A}_m^{-\frac{1}{2}}\right) = \mathrm{Tr}\left(\mathbf{A}_m^{-1}\mathbf{B}_m\right)$. Further, we have the following lemma on the structure of $\mathbf{C}_m$.

Lemma 1: All entries of $\mathbf{C}_m$ are zeros except for those in the first row, i.e., $c_{ij} = 0, \forall i \geq 2, j = 1 \cdots d$.

Proof: If there exists some $c_{i_0 j} \neq 0$ ($i_0 \geq 2$, $i_0 < j$), the i_0-th row and the first row must be linear independent. In other words, the rank of $\mathbf{C}_m$ is at least 2. This contradicts the prerequisite.

Let $\mathbf{U}_m^H \mathbf{A}_m^{-1} \mathbf{U}_m$ be partitioned as

$$\mathbf{U}_m^H \mathbf{A}_m^{-1} \mathbf{U}_m = \begin{bmatrix} t_{11} & \mathbf{t}_{21}^H \\ \mathbf{t}_{21} & \mathbf{T}_{22} \end{bmatrix}, \tag{12}$$

where $\mathbf{t}_{12} \in \mathbb{C}^{(d-1) \times 1}$ and $\mathbf{T}_{22} \in \mathbb{C}^{(d-1) \times (d-1)}$. With (12) and after a few manipulations, $q(\rho_m, \phi_m)$ can be finally expressed as

$$q(\rho_m, \phi_m) = \frac{\left[t_{11} + \mathrm{Tr}\left(\mathbf{T}_{22}\bar{\mathbf{c}}\bar{\mathbf{c}}^H\right)\right] - 2\rho_t \cos\left(\phi_m + \phi_t\right)}{\left(1 - \|\bar{\mathbf{c}}\|_F^2\right) + 2\rho_c \cos\left(\phi_m + \phi_c\right)} + \mathrm{Tr}\left(\mathbf{T}_{22}\right), \tag{13}$$

where $\bar{\mathbf{c}} = \rho_m e^{-j\phi_m} \begin{bmatrix} c_{12} & \cdots & c_{1d} \end{bmatrix}^H \in \mathbb{C}^{(d-1) \times 1}$, $\rho_t e^{j\phi_t} = \rho_m \begin{bmatrix} c_{12} & \cdots & c_{1d} \end{bmatrix} \mathbf{t}_{21}$, and $\rho_c e^{j\phi_c} = c_{11}$. The derivation of (13) is given by Appendix A.

Given ρ_m, the function $q(\rho_m, \phi_m)$ is a periodical function of ϕ_m. It is not difficult to find that, $q(\rho_m, \phi_m)$ has two extreme points within a period: one is the maximal point and the other is the minimal point. Clearly, the latter is the desired solution. By setting $\frac{\partial q(\rho_m, \phi_m)}{\partial \phi_m} = 0$, it can be derived that the minimal point is

$$\phi_m^\star = \arctan\left\{\frac{c_{st,1}\rho_c}{\rho_t c_{st,2}} + \cot\left(\phi_t - \phi_c\right)\right\}$$

$$+ \arccos\left\{-2\left[\left(\frac{c_{st,1}}{\rho_t \sin(\phi_t - \phi_c)} + \frac{\cot(\phi_t - \phi_c)c_{st,2}}{\rho_c}\right)^2 + \frac{c_{st,2}^2}{\rho_c^2}\right]^{-\frac{1}{2}}\right\} - \phi_c,$$

where $c_{st,1} = t_{11} + \mathrm{Tr}\left(\mathbf{T}_{22}\bar{\mathbf{c}}\bar{\mathbf{c}}^H\right)$ and $c_{st,2} = 1 - \|\bar{\mathbf{c}}\|_F^2$.

2) $\mathrm{Tr}\left(\mathbf{A}_m^{-1}\mathbf{B}_m\right) = 0$: In this case, $\mathrm{Tr}\left(\mathbf{A}_m^{-1}\mathbf{B}_m\right) = \mathrm{Tr}\left(\mathbf{A}_m^{-\frac{1}{2}}\mathbf{B}_m\mathbf{A}_m^{-\frac{1}{2}}\right) = 0$. If $\mathrm{rank}\left(\mathbf{A}_m^{-1}\mathbf{B}_m\right) = 0$, it follows that $\mathbf{A}_m^{-1}\mathbf{B}_m = \mathbf{A}_m^{-\frac{1}{2}}\mathbf{B}_m\mathbf{A}_m^{-\frac{1}{2}} = \mathbf{0}$ and any ϕ_m is optimal. Hence, we emphasize at the situation where $\mathrm{rank}\left(\mathbf{A}_m^{-1}\mathbf{B}_m\right) = \mathrm{rank}\left(\mathbf{A}_m^{-\frac{1}{2}}\mathbf{B}_m\mathbf{A}_m^{-\frac{1}{2}}\right) = 1$.

As it has rank one, $\mathbf{A}_m^{-\frac{1}{2}}\mathbf{B}_m\mathbf{A}_m^{-\frac{1}{2}}$ can be expressed as the product of two nonzero vectors $\mathbf{x}_m, \mathbf{y}_m \in \mathbb{C}^{d\times 1}$, i.e., $\mathbf{A}_m^{-\frac{1}{2}}\mathbf{B}_m\mathbf{A}_m^{-\frac{1}{2}}=\mathbf{x}_m\mathbf{y}_m^H$. For notation brevity, we use $\mathbf{x}$, $\mathbf{y}$ instead of $\mathbf{x}_m$, $\mathbf{y}_m$ in the subsequent derivations. With this formula, $q(\rho_m, \phi_m)$ in (10) is expressed as

$$q(\rho_m, \phi_m) = \mathrm{Tr}\left[\mathbf{A}_m^{-\frac{1}{2}}\left(\mathbf{I}_d + \rho_m e^{j\phi_m}\mathbf{x}\mathbf{y}^H + \rho_m e^{-j\phi_m}\mathbf{y}\mathbf{x}^H\right)^{-1}\mathbf{A}_m^{-\frac{1}{2}}\right]. \tag{14}$$

To further exploit the function $q(\rho_m, \phi_m)$, we introduce the Sherman-Morrison-Woodbury formula [38, Eq. (0.7.4.2)]: $\left(\mathbf{X} + \mathbf{a}\mathbf{b}^H\right)^{-1} = \mathbf{X}^{-1} - \frac{\mathbf{X}^{-1}\mathbf{a}\mathbf{b}^H\mathbf{X}^{-1}}{1+\mathbf{b}^H\mathbf{X}^{-1}\mathbf{a}}$. With this formula, one has $\left(\mathbf{I}_d + \rho_m e^{j\phi_m}\mathbf{x}\mathbf{y}^H\right)^{-1} = \mathbf{I}_d - \rho_m e^{j\phi_m}\mathbf{x}\mathbf{y}^H$ and

$$\left(\mathbf{I}_d + \rho_m e^{j\phi_m}\mathbf{x}\mathbf{y}^H + \rho_m e^{-j\phi_m}\mathbf{y}\mathbf{x}^H\right)^{-1}$$
$$= \left(\mathbf{I}_d + \rho_m e^{j\phi_m}\mathbf{x}\mathbf{y}^H\right)^{-1} - \frac{\left(\mathbf{I}_d+\rho_m e^{j\phi_m}\mathbf{x}\mathbf{y}^H\right)^{-1}\rho_m e^{-j\phi_m}\mathbf{y}\mathbf{x}^H\left(\mathbf{I}_d+\rho_m e^{j\phi_m}\mathbf{x}\mathbf{y}^H\right)^{-1}}{1+\rho_m e^{-j\phi_m}\mathbf{y}^H\left(\mathbf{I}_d+\rho_m e^{j\phi_m}\mathbf{x}\mathbf{y}^H\right)^{-1}\mathbf{x}}. \tag{15}$$

Noticing that $\mathrm{Tr}\left(\mathbf{A}_m^{-1}\mathbf{B}_m\right) = 0$ results in $\mathbf{y}^H\mathbf{x} = \mathbf{x}^H\mathbf{y} = 0$ and after a few manipulations, (15) can be finally expressed as

$$\left(\mathbf{I}_d + \rho_m e^{j\phi_m}\mathbf{x}\mathbf{y}^H + \rho_m e^{-j\phi_m}\mathbf{y}\mathbf{x}^H\right)^{-1}$$
$$= \mathbf{I}_d + \|\mathbf{x}\|_F^2\,\mathbf{y}\mathbf{y}^H + \|\mathbf{y}\|_F^2\,\mathbf{x}\mathbf{x}^H - \frac{\rho_m e^{j\phi_m}\mathbf{x}\mathbf{y}^H+\rho_m e^{-j\phi_m}\mathbf{y}\mathbf{x}^H}{1-\|\mathbf{x}\|_F^2\cdot\|\mathbf{y}\|_F^2}. \tag{16}$$

Substituting (16) into (14), one obtains

$$q(\rho_m, \phi_m) = \mathrm{Tr}\left[\mathbf{A}_m^{-1}\left(\mathbf{I}_d + \|\mathbf{x}\|_F^2\,\mathbf{y}\mathbf{y}^H + \|\mathbf{y}\|_F^2\,\mathbf{x}\mathbf{x}^H\right)\right]$$
$$-\frac{1}{1-\|\mathbf{x}\|_F^2\cdot\|\mathbf{y}\|_F^2}\mathrm{Tr}\left[\mathbf{A}_m^{-1}\left(\rho_m e^{j\phi_m}\mathbf{x}\mathbf{y}^H+\rho_m e^{-j\phi_m}\mathbf{y}\mathbf{x}^H\right)\right]$$
$$= c_{st,3} - \frac{2\rho_m}{1-\|\mathbf{x}\|_F^2\cdot\|\mathbf{y}\|_F^2}\mathrm{Re}\left\{e^{j\phi_m}\mathrm{Tr}\left(\mathbf{A}_m^{-2}\mathbf{B}_m\right)\right\},$$

where $c_{st,3} = \mathrm{Tr}\left[\mathbf{A}_m^{-1}\left(\mathbf{I}_d + \|\mathbf{x}\|_F^2\,\mathbf{y}\mathbf{y}^H + \|\mathbf{y}\|_F^2\,\mathbf{x}\mathbf{x}^H\right)\right]$. Clearly, given ρ_m, the optimal phase that minimizes $q(\rho_m, \phi_m)$ is $\phi_m^\star = -\arg\left[\mathrm{Tr}\left(\mathbf{A}_m^{-2}\mathbf{B}_m\right)\right]$, where $\arg[x]$ takes the angle of x.

To sum up, the optimal solution to $\min\limits_{\phi_m} q(\rho_m, \phi_m)$ is given by

$$\phi_m^\star = \begin{cases} -\arg\left[\mathrm{Tr}\left(\mathbf{A}_m^{-2}\mathbf{B}_m\right)\right], & \text{if } \mathrm{Tr}\left(\mathbf{A}_m^{-1}\mathbf{B}_m\right) = 0; \\ \arccos\left\{-2\left[\left(\frac{c_{st,1}}{\rho_t\sin(\phi_t-\phi_c)} + \frac{\cot(\phi_t-\phi_c)c_{st,2}}{\rho_c}\right)^2+\frac{c_{st,2}^2}{\rho_c^2}\right]^{-\frac{1}{2}}\right\} \\ \qquad + \arctan\left\{\frac{c_{st,1}\rho_c}{\rho_t c_{st,2}} + \cot\left(\phi_t-\phi_c\right)\right\} - \phi_c, & \text{else.} \end{cases} \tag{17}$$

Since $f_1(\rho_m) = \min\limits_{\phi_m} q(\rho_m, \phi_m)$ has been solved, $\mathrm{P}_{2\text{-m}}$ can be solved by one-dimensional line search of $f_1(\rho_m)$ over $0 \le \rho_m \le 1$. Subsequently, the method of successively optimizing reflection coefficients is summarized in *Algorithm 1.1*.

Finally, we briefly analyze the convergence and complexity of this algorithm. First, given m, the optimal solution to $\mathrm{P}_{2\text{-m}}$ is obtained from Step 2. Hence, this algorithm will generate

13

Algorithm 1.1: The proposed SORC algorithm for P_2.

Input: $\mathbf{F}, \mathbf{R}, \mathbf{T}, \mathbf{H}_0, \mathbf{R_n}, d, P_T$
Output: $\{\alpha_m\}_{i=1}^M$
 1: Randomly generate $\{\alpha_m = \rho_m e^{j\phi_m}\}_{i=1}^M$ with $0 \leq \rho_m \leq 1, \forall m$.
 2: **for** $m = 1$ to M **do**
    With (17), solve $P_{2\text{-m}}$ by one-dimensional line search of $f_1(\rho_m)$ over $0 \leq \rho_m \leq 1$. Denote
    $\alpha_m^\star = \rho_m^\star e^{j\phi_m^\star}$ as the optimal solution to $P_{2\text{-m}}$.
    Update $\alpha_m := \alpha_m^\star$.
   end for
 3: Repeat Steps 2-3 until convergence.

---

a series of non-increasing MSEs, i.e., the objective values of P_2. On the other hand, the MSE is lower bounded (larger than zero) and it follows that the algorithm converges. Moreover, considering that all α_m's are not coupled in P_2's constraints, the limit point generated by this algorithm satisfies the Karush-Kuhn-Tucker (KKT) condition of P_2 [39] and it is a KKT point. Second, for $\mathbf{X} \in \mathbb{C}^{n \times n}$, its Schur triangularization has the complexity of $\mathcal{O}(n^3)$. The computation of this algorithm mainly lies in Step 2, where the Schur triangularization and a few matrix multiplications are involved. The complexity of this algorithm can be summarized as $\mathcal{O}[I_1 I_2 M (d^3 + d^2 N_R + N_R N_T)]$, where I_1 is the outer iteration number and I_2 is the modulus samples' number in one-dimension search.

Remark 3: For the case where only the phase shifts can be tuned, i.e., $|\alpha_m| = 1, \forall m$, the optimal phase for $P_{2\text{-m}}$ can be solved by setting $\rho_m = |\alpha_m| = 1$ in (17). The proposed *Algorithm 1.1* is also available for P_2 with unit-modulus constraints for IRS coefficients except for a slight change. That is, solve $P_{2\text{-m}}$ by setting $\rho_m = 1$ in Step 2, instead of one-dimensional line search over $0 \leq \rho_m \leq 1$.

C. Overall Algorithm

In the previous subsection, we have proposed an algorithm to solve P_2. This subsection presents the complete alternating algorithm of solving P_1. As aforementioned, this algorithm iteratively solves the two subproblems in subsection *A*, which can be summarized in *Algorithm 1*.

Algorithm 1 is under the alternating optimization framework, and it is clear that the objective of P_1 is non-increasing with each iteration. Since the objective, larger than zero and hence lower

14

Algorithm 1: The proposed algorithm for P_1.

Input: R, T, H_0, R_n, d, P_T
Output: F, Φ, G
  1: Randomly generate $\{\alpha_m = \rho_m e^{j\phi_m}\}_{i=1}^M$ with $0 \le \rho_m \le 1, \forall m$.
  2: Given $\Phi = \text{diag}\{\alpha_1, \cdots, \alpha_M\}$, solve F according to (7).
  3: Given F, solve $\{\alpha_m\}_{i=1}^M$ by *Algorithm 1.1*.
  4: Repeat Steps 2-4 until convergence.
  5: Solve G by (5).

---

bounded, does not increase with the iteration number, *Algorithm 1* converges. Further, due to the fact that F and Φ are not coupled in P_1's constraints, the limit point by *Algorithm 1* is a stationary point of P_1. Besides, considering that the eigen-decomposition for $X \in \mathbb{C}^{n \times n}$ has the complexity of $\mathcal{O}(n)^3$, it can be shown that Step 2 has the complexity of $\mathcal{O}(MN_RN_T + N_R^2N_T + N_T^3)$. With the complexity analysis on *Algorithms 1.1* in the previous subsection, it can be found that *Algorithm 1* has the complexity of $\mathcal{O}\{I_{\Sigma,1}[I_1I_2M(d^3 + d^2N_R + N_RN_T) + N_R^2N_T + N_T^3]\}$, where $I_{\Sigma,1}$ is the outer iteration number.

D. Further Discussions

This subsection further explores problem P_1, in which we present the optimality condition for the IRS coefficient, study a few special cases, and discuss the group-based optimization scheme.

To begin with, we have the following proposition on the optimal α_m.

Proposition 1: If α_m satisfies (34) and $|\alpha_m| \le 1$, it is a candidate solution to $P_{2\text{-m}}$. Otherwise, the optimal α_m must satisfy $|\alpha_m| = 1$.

This proposition presents the optimality condition for α_m, the proof of which is given by Appendix B. With (17), we may first find a solution by setting $|\alpha_m| = 1$, denoted as $\bar{\alpha}_m$. Then, solve (34), obtaining another solution, denoted as $\hat{\alpha}_m$, and verify whether $\hat{\alpha}_m$ satisfies $|\hat{\alpha}_m| \le 1$. If this condition does not hold, the optimal solution to $P_{2\text{-m}}$ is $\bar{\alpha}_m$. Otherwise, choose a better one from $\bar{\alpha}_m$ and $\hat{\alpha}_m$ by comparing their objective values. Instead of 1D line search for the optimal α_m, *Proposition 1* provides another approach, where an equation in complex variable is involved and one may resort to the Newton-type iterative algorithm for complex variables [40].

Then, we study a few special cases.

1) Beamforming Transmission: In this case, the number of data stream $d = 1$ and the precoder matrix $\mathbf{F} \in \mathbb{C}^{N_T \times d}$ becomes a column vector. Given $\boldsymbol{\Phi}$, the optimal $\mathbf{F} = \sqrt{P_T}\mathbf{u}_{\text{BF}}$, where $\mathbf{u}_{\text{BF}} \in \mathbb{C}^{N_T \times 1}$ is the eigenvector of $\mathbf{H}^H \mathbf{R}_\mathbf{n}^{-1} \mathbf{H}$ corresponding to the largest eigenvalue. Given $\mathbf{F}$, with (9), the objective of $\text{P}_{2\text{-m}}$ is

$$q(\rho_m, \phi_m) = \left[1 + \left(\tilde{\mathbf{H}}_0 + \sum_{i=1, i \neq m}^{M} \alpha_i \tilde{\mathbf{r}}_i \tilde{\mathbf{t}}_i^T \right)^H \left(\tilde{\mathbf{H}}_0 + \sum_{i=1, i \neq m}^{M} \alpha_i \tilde{\mathbf{r}}_i \tilde{\mathbf{t}}_i^T \right) \right.$$
$$\left. + |\alpha_m|^2 \left(\tilde{\mathbf{r}}_m \tilde{\mathbf{t}}_m^T \right)^H \left(\tilde{\mathbf{r}}_m \tilde{\mathbf{t}}_m^T \right) + \alpha_m \mathbf{B}_m + \alpha_m^* \mathbf{B}_m^H \right]^{-1},$$

where $\alpha_m \triangleq \rho_m e^{j\phi_m}$. Clearly, $\min q(\rho_m, \phi_m)$ is equivalent to $\max |\alpha_m|^2 (\tilde{\mathbf{r}}_m \tilde{\mathbf{t}}_m^T)^H (\tilde{\mathbf{r}}_m \tilde{\mathbf{t}}_m^T) + \alpha_m \mathbf{B}_m + \alpha_m^* \mathbf{B}_m^H$. The optimal solution can be shown to be $\rho_m^\star = 1, \phi_m^\star = -\arg\{\mathbf{B}_m\}$.

2) MISO/SIMO: We consider the MISO case. Given $\boldsymbol{\Phi}$, the optimal $\mathbf{F} = \sqrt{P_T}\mathbf{u}_{\text{MISO}}$, where $\mathbf{u}_{\text{MISO}} \in \mathbb{C}^{N_T \times 1}$ is the eigenvector of $\mathbf{H}^H \mathbf{R}_\mathbf{n}^{-1} \mathbf{H}$ corresponding to the unique nonzero eigenvalue. Given $\mathbf{F}$, the objective of $\text{P}_{2\text{-m}}$ is

$$q(\rho_m, \phi_m) = \text{Tr}\left[\left(\mathbf{I}_d + \mathbf{F}^H \mathbf{H}^H \mathbf{R}_\mathbf{n}^{-1} \mathbf{H} \mathbf{F} \right)^{-1} \right]$$
$$= \text{Tr}\left[\left(1 + \mathbf{H} \mathbf{F} \mathbf{R}_\mathbf{n}^{-1} \mathbf{F}^H \mathbf{H}^H \right)^{-1} \right] + d - 1$$
$$= \left(1 + \mathbf{H} \mathbf{F} \mathbf{R}_\mathbf{n}^{-1} \mathbf{F}^H \mathbf{H}^H \right)^{-1} + d - 1$$
$$= \left[\mathbf{A}'_m + \alpha_m \mathbf{B}'_m + \alpha_m^* (\mathbf{B}'_m)^H \right]^{-1},$$

where $\mathbf{A}'_m = 1 + \left(\tilde{\mathbf{H}}_0 + \sum_{i=1, i \neq m}^{M} \alpha_i \tilde{\mathbf{r}}_i \tilde{\mathbf{t}}_i^T \right) \left(\tilde{\mathbf{H}}_0 + \sum_{i=1, i \neq m}^{M} \alpha_i \tilde{\mathbf{r}}_i \tilde{\mathbf{t}}_i^T \right)^H + |\alpha_m|^2 (\tilde{\mathbf{r}}_m \tilde{\mathbf{t}}_m^T)(\tilde{\mathbf{r}}_m \tilde{\mathbf{t}}_m^T)^H$ and $\mathbf{B}'_m = \tilde{\mathbf{r}}_m \tilde{\mathbf{t}}_m^T (\tilde{\mathbf{H}}_0 + \sum_{i=1, i \neq m}^{M} \alpha_i \tilde{\mathbf{r}}_i \tilde{\mathbf{t}}_i^T)^H$. The optimal solution can be shown as $\rho_m^\star = 1, \phi_m^\star = -\arg\{\mathbf{B}'_m\}$. In addition, similar analysis can be conducted on the SIMO case, which is omitted for brevity.

Finally, we discuss the group-based optimization scheme. The group-based IRS optimization strategy was proposed in [41], where the IRS units were partitioned into several groups and then optimized in two stages. This scheme is quite effective for large IRSs by exploiting the tradeoff between complexity and performance. Here, we borrow this concept and preliminarily explore the group-based optimization. Divide M elements into N_G groups and each group has M/N_G elements. The effective channel is rewritten as

$$\mathbf{H} = \mathbf{H}_0 + \sum_{m=1}^{M} \alpha_m \mathbf{r}_m \mathbf{t}_m^T = \mathbf{H}_0 + \sum_{i=1}^{N_G} \beta_i^G \left(\sum_{j=1}^{M/N_G} \beta_{ij}^g \mathbf{r}_m \mathbf{t}_m^T \right),$$

where $\alpha_m = \beta_i^G \beta_{ij}^g$ with $m = (i-1)\frac{M}{N_G} + j$, β_i^G is the intergroup coefficient for group i, and

16

β_{ij}^g is the intragroup coefficient for element j in group i. We further assume that only one set of intragroup coefficients is used, i.e., $\beta_{ij}^g = \beta_{1j}^g, \forall i$. In this way, only two sets, $\{\beta_i^G\}_{i=1}^{N_G}$ and $\{\beta_{1j}^g\}_{j=1}^{\frac{M}{N_G}}$, need to be optimized, and the number of optimization variables is $N_G + M/N_G$. The group-based optimization is still under the framework of alternating optimization, i.e., two sets are optimized alternately. For optimizing one set of variables, each time we only optimize one single variable with others being fixed. The details are omitted for brevity.

Besides, there is a simpler group-based scheme, where $\beta_{ij}^g = 1, \forall i, j$, i.e., the intragroup coefficients are assumed to be identical. Hence, only $\{\beta_i^G\}_{i=1}^{N_G}$ needs to be optimized and the number of optimization variables is reduced to N_G. The performance of both schemes will be evaluated by computer simulation.

IV. Joint Precoder, Reflection Coefficients, and Equalizer Design with Imperfect CSI

In the previous section, we have optimized the linear transceiver and reflection coefficients under the assumption that the system has perfect CSI. Specifically, the direct channel matrix $\mathbf{H}_0$ is exactly known; either the two matrices $\mathbf{R}, \mathbf{T}$ or the cascaded matrices $\mathbf{r}_m \mathbf{t}_m^T, \forall m$ are exactly known. However, in practice, it is difficult to obtain perfect CSI due to the followings: 1) The channel noise and Doppler effect reduce the quality of channel estimation; 2) for an IRS-aided system, the available pilots appear insufficient due to the large number of IRS elements; 3) the pilot contamination due to intra/inter-IRS interference is also a negative factor. In this situation, robust design in which the channel uncertainties are considered is of significance since it can reduce the performance degradation and enhance the robustness of the system. Assuming that only imperfect CSI is available for the system (i.e., both the transmitter and receiver), this section studies the robust joint transceiver and IRS design against the CSI error.

A. Channel Error Model

This subsection presents a more generalized channel error model, where the mean and covariance matrices of the channel error are specified, but the distribution is not.

We borrow the error model from the existing literature [42]–[44], in which the channel spatial correlation is incorporated. Specifically, the estimation error matrix is modeled by

$$\Delta \mathbf{H}' = \Theta_{\mathrm{B}}^{\frac{1}{2}} \mathbf{H}_\omega' \Theta_{\mathrm{A}}^{\frac{1}{2}}, \tag{18}$$

where $\boldsymbol{\Theta}_A$ and $\boldsymbol{\Theta}_B$ are the row and column covariance matrices of $\Delta \mathbf{H}'$, respectively; $\mathbf{H}'_\omega$ consists of *i.i.d* complex Gaussian random variables with zero mean and unit variance. With (18), it follows that $\operatorname{vec}\left((\Delta \mathbf{H}')^T\right) \sim \mathcal{CN}\left(\mathbf{0}, \boldsymbol{\Theta}_B \otimes \boldsymbol{\Theta}_A^T\right)$, where $\operatorname{vec}(\cdot)$ denotes the vectorization operation and $\otimes$ is the Kronecker product. As will be seen later, the derivation of MSE is only related with two covariance matrices $\boldsymbol{\Theta}_A$, $\boldsymbol{\Theta}_B$, and hence we generalize the model (18) by not limiting the distribution of $\operatorname{vec}\left[(\Delta \mathbf{H}')^T\right]$. In other words, the elements of $\mathbf{H}'_\omega$ are not limited to Gaussian distribution and $\operatorname{vec}\left[(\Delta \mathbf{H}')^T\right] \sim \mathcal{F}\left(\mathbf{0}, \boldsymbol{\Theta}_B \otimes \boldsymbol{\Theta}_A^T\right)$, where $\mathcal{F}(\cdot)$ denotes some distribution.

Based on the above, the estimated direct channel matrix is modeled by $\widehat{\mathbf{H}}_0 = \mathbf{H}_0 + \Delta \mathbf{H}_0$, with $\operatorname{vec}\left[(\Delta \mathbf{H}_0)^T\right] \sim \mathcal{F}_0\left(\mathbf{0}, \boldsymbol{\Theta}_{B,0} \otimes \boldsymbol{\Theta}_{A,0}^T\right)$. On the other front, the cascaded channel, the product of the transmit-IRS channel and IRS-receive channel, is often sufficient and used for the joint design in IRS-aided systems [4], [6]. The robust joint design is based on the estimated cascaded channels, which are modeled as $\widehat{\mathbf{L}}_m = \mathbf{L}_m + \Delta \mathbf{L}_m, \forall m$, where $\mathbf{L}_m \in \mathbb{C}^{N_R \times N_T} \triangleq \mathbf{r}_m \mathbf{t}_m^T$, $\widehat{\mathbf{L}}_m$ is the estimated $\mathbf{L}_m$, and

$$\operatorname{vec}\left[(\Delta \mathbf{L}_m)^T\right] \sim \mathcal{F}_m\left(\mathbf{0}, \boldsymbol{\Theta}_{B,m} \otimes \boldsymbol{\Theta}_{A,m}^T\right).$$

The estimation for $\mathbf{L}_m$'s can be successively conducted [45]–[47] so that $\Delta \mathbf{L}_m$'s are independent. Furthermore, with (1), it can be verified that the covariance matrices of $\mathbf{L}_m$ are independent of m. Since the covariance matrices of $\Delta \mathbf{L}_m$ are closely related with that of $\mathbf{L}_m$, we can further assume that $\boldsymbol{\Theta}_{A,m}$ and $\boldsymbol{\Theta}_{B,m}$ do not depend on m, i.e.,

$$\boldsymbol{\Theta}_{A,m} = \boldsymbol{\Theta}_{A,\mathrm{IRS}}, \boldsymbol{\Theta}_{B,m} = \boldsymbol{\Theta}_{B,\mathrm{IRS}}, \forall m.$$

Take an example. If the conventional minimum MSE (MMSE) method [42] is adopted to estimate the cascaded channel, we have $\boldsymbol{\Theta}_{A,m} = \boldsymbol{\Theta}_{A,\mathrm{IRS}} = g_1 g_2 \sigma_e^2 \left(\mathbf{I}_{N_R} + \sigma_e^2 \boldsymbol{\Psi}_{R,2}^{-1}\right)^{-1}$ and $\boldsymbol{\Theta}_{B,m} = \boldsymbol{\Theta}_{B,\mathrm{IRS}} = \boldsymbol{\Psi}_{T,1}, \forall m$, where σ_e^2 is the normalized estimation error variance.

In this way, the equivalent channel matrix with uncertainties can be written as

$$\mathbf{H} = \mathbf{H}_0 + \sum_{m=1}^{M} \alpha_m \mathbf{r}_m \mathbf{t}_m^T = \widehat{\mathbf{H}} + \Delta \mathbf{H}, \tag{19}$$

where $\widehat{\mathbf{H}} = \widehat{\mathbf{H}}_0 + \sum_m \alpha_m \widehat{\mathbf{L}}_m$ and $\Delta \mathbf{H} = \Delta \mathbf{H}_0 + \sum_m \alpha_m \Delta \mathbf{L}_m$.

Note that, in [48], the equivalent channel between an AP and a user was estimated, where the IRS phase shifts were optimized based on the statistical CSI. While in this paper, the IRS coefficients are optimized based on the instantaneous CSI, i.e., the MSE is minimized

18

by optimizing the IRS coefficients based on the instantaneous estimated CSI. Therefore, the estimated CSI can not contain the information of IRS coefficients and the estimation for cascaded channels is suitable.

B. Problem Formulation

To overcome the impact of the statistical CSI error, we optimize the average MSE over channel uncertainties, which is a commonly-used approach for stochastic channels [49]. The overall logical flow is as follows. The first step is to derive the expected MSE expression over channel uncertainties. Next, the equalizer $\mathbf{G}$ is optimized so that the MSE expression is simplified and becomes a function of only two variables: $\mathbf{F}$ and $\boldsymbol{\Phi}$. Then, with the aid of a matrix inequality, we derive the upper bound of MSE. In this way, we will optimize the MSE indirectly by minimizing the MSE upper bound.

First, with the channel error model, we derive the expected MSE expression over $\mathbf{n}$, $\mathbf{s}$, and $\Delta\mathbf{H}$. The MSE in (3) is further expressed as

$$
\begin{aligned}
\text{MSE} &= \mathbb{E}_{\mathbf{n},\mathbf{s},\Delta\mathbf{H}} \left\{ \text{Tr} \left[(\mathbf{GHFs} + \mathbf{Gn} - \mathbf{s}) (\mathbf{GHFs} + \mathbf{Gn} - \mathbf{s})^H \right] \right\} \\
&= \mathbb{E}_{\Delta\mathbf{H}} \left\{ \text{Tr} \left[(\mathbf{GHF} - \mathbf{I}_d) (\mathbf{GHF} - \mathbf{I}_d)^H \right] \right\} + \text{Tr} \left[\mathbf{GR_n G}^H \right].
\end{aligned}
\tag{20}
$$

Substituting (19) into (20), one obtains

$$
\text{MSE} = \text{Tr} \left[\left(\mathbf{G\hat{H}F} - \mathbf{I}_d \right) \left(\mathbf{G\hat{H}F} - \mathbf{I}_d \right)^H \right] + \text{Tr} \left[\mathbf{GR_n G}^H \right] + \mathbb{E}_{\Delta\mathbf{H}} \left\{ \text{Tr} \left[(\mathbf{G\Delta HF})^H (\mathbf{G\Delta HF}) \right] \right\}. \tag{21}
$$

The third item on the right side of (21) is derived as

$$
\begin{aligned}
&\mathbb{E}_{\Delta\mathbf{H}} \left\{ \text{Tr} \left[(\mathbf{G\Delta HF})^H (\mathbf{G\Delta HF}) \right] \right\} \\
&= \text{Tr} \left[\mathbf{G} \mathbb{E}_{\Delta\mathbf{H}} \left(\Delta\mathbf{HFF}^H \Delta\mathbf{H}^H \right) \mathbf{G}^H \right] \\
&= \text{Tr} \left\{ \mathbf{G} \mathbb{E}_{\Delta\mathbf{H}} \left[\left(\Delta\mathbf{H}_0 + \sum_{m=1}^{M} \alpha_m \Delta\mathbf{L}_m \right) \mathbf{FF}^H \left(\Delta\mathbf{H}_0 + \sum_{m=1}^{M} \alpha_m \Delta\mathbf{L}_m \right)^H \right] \mathbf{G}^H \right\} \\
&= \text{Tr} \left\{ \mathbf{G} \left[\text{Tr} \left(\mathbf{FF}^H \boldsymbol{\Theta}_{\text{B},0} \right) \boldsymbol{\Theta}_{\text{A},0} + \sum_m |\alpha_m|^2 \text{Tr} \left(\mathbf{FF}^H \boldsymbol{\Theta}_{\text{B,IRS}} \right) \boldsymbol{\Theta}_{\text{A,IRS}} \right] \mathbf{G}^H \right\}.
\end{aligned}
\tag{22}
$$

With (22), the MSE in (21) can be finally written as

$$
\text{MSE} = \text{Tr} \left[\mathbf{G}(\mathbf{K} + \mathbf{\hat{H}FF}^H \mathbf{\hat{H}}^H) \mathbf{G}^H \right] + d - \text{Tr} \left(\mathbf{G\hat{H}F} \right) - \text{Tr} \left(\mathbf{G\hat{H}F} \right)^H, \tag{23}
$$

where

$$
\mathbf{K} \triangleq \mathbf{R_n} + \text{Tr} \left(\mathbf{FF}^H \boldsymbol{\Theta}_{\text{B},0} \right) \boldsymbol{\Theta}_{\text{A},0} + \sum_m |\alpha_m|^2 \text{Tr} \left(\mathbf{FF}^H \boldsymbol{\Theta}_{\text{B,IRS}} \right) \boldsymbol{\Theta}_{\text{A,IRS}}. \tag{24}
$$

Next, we consider the optimization of the equalizer $\mathbf{G}$. Since the design problem does not impose constraints on $\mathbf{G}$, the optimal $\mathbf{G}$ can be solved by setting $\frac{\partial \text{MSE}}{\partial \mathbf{G}^*} = \mathbf{0}$. It is easy to find that the optimal $\mathbf{G}$ is

$$\mathbf{G}^{\text{OPT}} = (\widehat{\mathbf{H}}\mathbf{F})^H (\mathbf{K} + \widehat{\mathbf{H}}\mathbf{F}\mathbf{F}^H \widehat{\mathbf{H}}^H)^{-1}. \tag{25}$$

Substituting (25) into (23), after a few manipulations we have

$$\text{MSE}(\mathbf{F}, \boldsymbol{\Phi}) = \text{Tr}\left[\left(\mathbf{I}_d + \mathbf{F}^H \widehat{\mathbf{H}}^H \mathbf{K}^{-1} \widehat{\mathbf{H}}\mathbf{F}\right)^{-1}\right], \tag{26}$$

in which we write $\text{MSE} = \text{MSE}(\mathbf{F}, \boldsymbol{\Phi})$ to emphasize that MSE is a function of $\mathbf{F}$ and $\boldsymbol{\Phi}$.

Then, observe from (26) that, minimizing $\text{MSE}(\mathbf{F}, \boldsymbol{\Phi})$ is intractable due to the matrix $\mathbf{K}$. To handle the problem, we derive $\mathbf{K}$'s upper bound and obtain MSE's upper bound afterwards. With (24) and [38, Theorem 4.2.2],

$$\begin{aligned}
\mathbf{K} &= \mathbf{R_n}^{\frac{1}{2}} \left[\mathbf{I}_{N_R} + \text{Tr}\left(\mathbf{F}\mathbf{F}^H \boldsymbol{\Theta}_{\text{B},0}\right) \mathbf{R_n}^{-\frac{1}{2}} \boldsymbol{\Theta}_{\text{A},0} \mathbf{R_n}^{-\frac{1}{2}} \right. \\
&\qquad\left. + \sum_m |\alpha_m|^2 \text{Tr}\left(\mathbf{F}\mathbf{F}^H \boldsymbol{\Theta}_{\text{B,IRS}}\right) \mathbf{R_n}^{-\frac{1}{2}} \boldsymbol{\Theta}_{\text{A,IRS}} \mathbf{R_n}^{-\frac{1}{2}}\right] \mathbf{R_n}^{1/2} \\
&\preceq \mathbf{R_n}^{\frac{1}{2}} \left[\mathbf{I}_{N_R} + \text{Tr}\left(\mathbf{F}\mathbf{F}^H \boldsymbol{\Theta}_{\text{B},0}\right) \lambda_{\text{A},0}^{\max} \cdot \mathbf{I}_{N_R} \right. \\
&\qquad\left. + \sum_m |\alpha_m|^2 \text{Tr}\left(\mathbf{F}\mathbf{F}^H \boldsymbol{\Theta}_{\text{B,IRS}}\right) \lambda_{\text{A,IRS}}^{\max} \cdot \mathbf{I}_{N_R}\right] \mathbf{R_n}^{1/2} \\
&= \mathbf{R_n} \left[1 + \text{Tr}\left(\mathbf{F}\mathbf{F}^H \boldsymbol{\Theta}_{\text{B},0}\right) \lambda_{\text{A},0}^{\max} + \sum_m |\alpha_m|^2 \text{Tr}\left(\mathbf{F}\mathbf{F}^H \boldsymbol{\Theta}_{\text{B,IRS}}\right) \lambda_{\text{A,IRS}}^{\max}\right],
\end{aligned} \tag{27}$$

where $\lambda_{\text{A},0}^{\max}$ and $\lambda_{\text{A,IRS}}^{\max}$ are the maximum eigenvalues of $\mathbf{R_n}^{-\frac{1}{2}} \boldsymbol{\Theta}_{\text{A},0} \mathbf{R_n}^{-\frac{1}{2}}$ and $\mathbf{R_n}^{-\frac{1}{2}} \boldsymbol{\Theta}_{\text{A,IRS}} \mathbf{R_n}^{-\frac{1}{2}}$, respectively. Substituting $\mathbf{K}$'s upper bound into (26), we have an upper bound of $\text{MSE}(\mathbf{F}, \boldsymbol{\Phi})$:

$$\begin{aligned}
&\text{MSE}^{\text{UP}}(\mathbf{F}, \boldsymbol{\Phi}) \\
&= \text{Tr}\left[\left(\mathbf{I}_d + \frac{\mathbf{F}^H \widehat{\mathbf{H}}^H \mathbf{R_n}^{-1} \widehat{\mathbf{H}}\mathbf{F}}{\left[1 + \text{Tr}\left(\mathbf{F}\mathbf{F}^H \boldsymbol{\Theta}_{\text{B},0}\right) \lambda_{\text{A},0}^{\max} + \sum_m |\alpha_m|^2 \text{Tr}\left(\mathbf{F}\mathbf{F}^H \boldsymbol{\Theta}_{\text{B,IRS}}\right) \lambda_{\text{A,IRS}}^{\max}\right]}\right)^{-1}\right].
\end{aligned} \tag{28}$$

Finally, for the joint design, we would like to optimize $\text{MSE}^{\text{UP}}(\mathbf{F}, \boldsymbol{\Phi})$ instead of $\text{MSE}(\mathbf{F}, \boldsymbol{\Phi})$. The design problem can be formulated as

$$\text{P}_3 : \min_{\mathbf{F}, \boldsymbol{\Phi}} \text{MSE}^{\text{UP}}(\mathbf{F}, \boldsymbol{\Phi})$$

$$s.t. \ C_1 \sim C_3$$

For P_3, it can be verified that the optimal $\mathbf{F}$ satisfies $\text{Tr}\left(\mathbf{F}\mathbf{F}^H\right) = P_T$. This can be proved by using reduction to absurdity and the proof is omitted for brevity. Using this fact, P_3 can be equivalently written as

20

$$\min_{\mathbf{F}, \boldsymbol{\Phi}} \ \mathrm{MSE}^{\mathrm{UP}}(\mathbf{F}, \boldsymbol{\Phi})$$

$$s.t. \ C_1' : \mathrm{Tr}\left(\mathbf{F}\mathbf{F}^H\right) = P_T$$

$$C_2, C_3.$$

C. The Proposed Algorithm

Similar to the previous section III, the proposed algorithm is also under the framework of alternating optimization, in which P_3 is divided into two subproblems being treated alternately.

1) Optimizing $\mathbf{F}$ given $\boldsymbol{\Phi}$: We define $\mathbf{D} = \mathbf{I}_{N_T}/P_T + \lambda_{\mathrm{A},0}^{\max}\boldsymbol{\Theta}_{\mathrm{B},0} + \lambda_{\mathrm{A,IRS}}^{\max} \sum_m |\alpha_m|^2 \boldsymbol{\Theta}_{\mathrm{B,IRS}}$ and write $\mathrm{MSE}^{\mathrm{UP}}(\mathbf{F}, \boldsymbol{\Phi})$ as another form: $\mathrm{MSE}^{\mathrm{UP}}(\mathbf{F}, \boldsymbol{\Phi}) = \mathrm{Tr}\left[\left(\mathbf{I}_d + \frac{\mathbf{F}^H\widehat{\mathbf{H}}^H\mathbf{R_n}^{-1}\widehat{\mathbf{H}}\mathbf{F}}{\mathrm{Tr}(\mathbf{F}^H\mathbf{D}\mathbf{F})}\right)^{-1}\right]$. Let

$\bar{\mathbf{F}} = \dfrac{\mathbf{D}^{\frac{1}{2}}\mathbf{F}}{\sqrt{\mathrm{Tr}(\mathbf{F}^H\mathbf{D}\mathbf{F})}}$. Given $\boldsymbol{\Phi}$, the subproblem of solving $\mathbf{F}$ can be formulated as

$$\mathrm{P}_{3\text{-}1} : \min_{\mathbf{F}, \bar{\mathbf{F}}} \ \mathrm{MSE}^{\mathrm{UP}}(\bar{\mathbf{F}}, \boldsymbol{\Phi}) = \mathrm{Tr}\left[\left(\mathbf{I}_d + \bar{\mathbf{F}}^H\mathbf{D}^{-\frac{1}{2}}\widehat{\mathbf{H}}^H\mathbf{R_n}^{-1}\mathbf{D}^{-\frac{1}{2}}\widehat{\mathbf{H}}\bar{\mathbf{F}}\right)^{-1}\right]$$

$$s.t. \ C_1' : \mathrm{Tr}\left(\mathbf{F}\mathbf{F}^H\right) = P_T$$

$$C_4 : \bar{\mathbf{F}} = \frac{\mathbf{D}^{\frac{1}{2}}\mathbf{F}}{\sqrt{\mathrm{Tr}(\mathbf{F}^H\mathbf{D}\mathbf{F})}}$$

Concerning $\mathrm{P}_{3\text{-}1}$, we have the following lemma.

Lemma 2: $\mathrm{P}_{3\text{-}1}$ is equivalent to the problem

$$\mathrm{P}_{3\text{-}1}' : \min_{\bar{\mathbf{F}}} \ \mathrm{MSE}^{\mathrm{UP}}(\bar{\mathbf{F}}, \boldsymbol{\Phi}) = \mathrm{Tr}\left[\left(\mathbf{I}_d + \bar{\mathbf{F}}^H\mathbf{D}^{-\frac{1}{2}}\widehat{\mathbf{H}}^H\mathbf{R_n}^{-1}\mathbf{D}^{-\frac{1}{2}}\widehat{\mathbf{H}}\bar{\mathbf{F}}\right)^{-1}\right]$$

$$s.t. \ \mathrm{Tr}\left(\bar{\mathbf{F}}\bar{\mathbf{F}}^H\right) = 1.$$

Proof: See Appendix C.

Since the matrix $\mathbf{D}^{-\frac{1}{2}}\widehat{\mathbf{H}}^H\mathbf{R_n}^{-1}\mathbf{D}^{-\frac{1}{2}}\widehat{\mathbf{H}}$ is positive semidefinite, $\mathrm{P}_{3\text{-}1}'$ is the same with the problem [37, Theorem 1] in form so that the closed-form solution to $\mathrm{P}_{3\text{-}1}'$, denoted as $\bar{\mathbf{F}}^\star$, can be solved. Here, the details are omitted for brevity. When $\mathrm{P}_{3\text{-}1}'$ is solved, the optimal $\mathbf{F}$ can be readily given by

$$\mathbf{F}^\star = \sqrt{P_T}\mathbf{D}^{-\frac{1}{2}}\bar{\mathbf{F}}^\star \Big/ \sqrt{\mathrm{Tr}\left(\left(\bar{\mathbf{F}}^\star\right)^H\mathbf{D}^{-1}\bar{\mathbf{F}}^\star\right)}. \tag{29}$$

2) Optimizing $\boldsymbol{\Phi}$ given $\mathbf{F}$: Given $\{\alpha_i, i \neq m\}_{i=1}^M$, consider the following problem

$$\mathrm{P}_{3\text{-}2\text{-}m} : \min_{0 \le \rho_m \le 1} f_2\left(\rho_m\right),$$

where

$$f_2\left(\rho_m\right) = \min_{\phi_m} \ \mathrm{MSE}^{\mathrm{UP}} = \mathrm{Tr}\left[\left(\mathbf{I}_d + \mathbf{F}^H\widehat{\mathbf{H}}^H\bar{\mathbf{R}}_\mathbf{n}^{-1}\widehat{\mathbf{H}}\mathbf{F}\right)^{-1}\right], \tag{30}$$

$\alpha_m \triangleq \rho_m e^{j\phi_m}$, and $\bar{\mathbf{R}}_{\mathbf{n}} = \mathbf{R_n} \text{Tr} \left(\mathbf{F}^H \mathbf{D} \mathbf{F} \right)$. Notice that the matrix $\mathbf{D}$ does not involve ϕ_m and hence can be treated as a constant when optimizing ϕ_m. Consequently, only $\widehat{\mathbf{H}}$ involves ϕ_m. We may arrange the objective of (30) as the form similar to (9) and solve the optimal ϕ_m by (17). Then, the optimal ρ_m can be solved by one-dimensional line search of $f_2 \left(\rho_m \right)$ over $0 \leq \rho_m \leq 1$. In a word, the whole processing is similar to *Algorithm 1.2*, the details of which are omitted.

Based on the above, the overall algorithm of solving P_3 is proposed and summarized in *Algorithm 2*. Similar to the convergence analysis on *Algorithm 1*, *Algorithm 2* also converges and the limit point generated by this algorithm is a stationary point of P_3. Besides, it can be shown that the computational complexity of this algorithm is $\mathcal{O}\{I_{\Sigma,2}[I_3 I_4 M(d^3 + d^2 N_R + N_R N_T) + N_R^2 N_T + N_T^3]\}$, where $I_{\Sigma,2}$ is the outer iteration number; I_3 and I_4 are the iteration number and the modulus samples' number in Step 3, respectively.

Algorithm 2: The proposed algorithm for P_3.

Input: $\widehat{\mathbf{R}}, \widehat{\mathbf{T}}, \widehat{\mathbf{H}}_0, \mathbf{R_n}, \mathbf{\Theta}_{\text{A},0}, \mathbf{\Theta}_{\text{B},0}, \mathbf{\Theta}_{\text{A,IRS}}, \mathbf{\Theta}_{\text{B,IRS}}, d, P_T$
Output: $\mathbf{F}, \mathbf{\Phi}, \mathbf{G}$
1: Randomly generate $\{\alpha_m = \rho_m e^{j\phi_m}\}_{i=1}^M$ with $0 \leq \rho_m \leq 1, \forall m$.
2: Given $\mathbf{\Phi} = \text{diag}\{\alpha_1, \cdots, \alpha_M\}$, solve $P'_{3\text{-}1}$ and obtain $\bar{\mathbf{F}}^\star$. Then, compute $\mathbf{F}$ by (29).
3: Given $\mathbf{F}$, solve $\{\alpha_m\}_{i=1}^M$ by the similar algorithm to *Algorithm 1.1*.
4: Repeat Steps 2-4 until convergence.
5: Solve $\mathbf{G}$ by (25).

V. SIMULATION RESULTS

In this section, computer simulation is deployed to investigate the performance of the proposed algorithms. Consider an IRS-assisted MIMO system with $N_T = N_R = 4$. Assume that both the transmitter and receiver are equipped with a uniform linear array (ULA) while the IRS is with a uniform planar array (UPA).

For the ULA, the (m, n)-th entry of the spatial correlation matrix $\mathbf{\Psi}_{\text{ULA}}$ is modeled as [33, Eq. (19)]

$$[\mathbf{\Psi}_{\text{ULA}}]_{m,n} = \gamma_0 \frac{\exp\left[j 2\pi \frac{d_A}{\lambda}(m-n)\sin\theta_0\right]}{1 + \frac{\sigma_\theta^2}{2}\left[2\pi \frac{d_A}{\lambda}(m-n)\cos\theta_0\right]},$$

where θ_0 the mean angle of arrival (AOA)/departure (AOD), σ_θ is the standard deviation of the power azimuth spectrum (PAS), d_A is the antenna spacing, λ is the wave length, and $\gamma_0 = \frac{1}{1 - \exp\left(-\frac{2\pi}{\sigma_\theta}\right)}$ is a normalization factor. The antenna spacing d_A is set to the half-wavelength

22

$\lambda/2$. The tuples $\{\theta_0, \sigma_\theta\}$'s are set to $\left\{\frac{\pi}{3}, \frac{\pi}{10}\right\}$, $\left\{\frac{\pi}{4}, \frac{\pi}{10}\right\}$, $\left\{\frac{\pi}{6}, \frac{\pi}{5}\right\}$, and $\left\{\frac{\pi}{4}, \frac{\pi}{10}\right\}$ for the correlation matrices $\boldsymbol{\Psi}_{R,0}$, $\boldsymbol{\Psi}_{T,0}$, $\boldsymbol{\Psi}_{R,2}$, and $\boldsymbol{\Psi}_{T,1}$, respectively.

For the UPA, the (m, n)-th entry of the spatial correlation matrix $\boldsymbol{\Psi}_{\mathrm{UPA}}$ is modeled as [50]

$$
\begin{aligned}
{[\boldsymbol{\Psi}_{\mathrm{UPA}}]_{m,n}} = \gamma_1 \int_{\theta=0}^{\frac{\pi}{2}} \int_{\varphi=\varphi_0-\pi}^{\varphi_0+\pi} & f_{\mathrm{elev}}\left(\theta\right) f_{\mathrm{azim}}\left(\varphi\right) \sin\theta \\
& \times \exp\left[j2\pi\left(i_1 - i_2\right) \frac{d_y}{\lambda} \sin\theta \sin\varphi\right] \\
& \times \exp\left[j2\pi\left(j_1 - j_2\right) \frac{d_x}{\lambda} \sin\theta \cos\varphi\right] d\theta d\varphi
\end{aligned}
,
$$

where $i_1 = \left\lfloor \frac{m}{M_x} \right\rfloor$, $j_1 = m - M_x i_1$, $i_2 = \left\lfloor \frac{n}{M_x} \right\rfloor$, and $j_2 = n - M_x i_2$, with M_x being the number of IRS elements in each row along the x-th axis; θ_0 and φ_0 are the mean azimulth and elevation angles, respectively; d_x and d_y are the IRS element spacings on the x-th axis and y-th axis, respectively; γ_1 is a normalized factor; $f_{\mathrm{elev}}\left(\theta\right)$ is the probability density function (PDF) of the elevation angle, which follows the truncated Laplacian distribution [50, Eq. (1)]; $f_{\mathrm{azim}}\left(\varphi\right)$ is the PDF of the azimuth angle, following the Von-Mises distribution [50, Eq. (5)]. In the simulation, the IRS element spacings d_x and d_y are both set to $\lambda/2$. For $\boldsymbol{\Psi}_{R,1}$ and $\boldsymbol{\Psi}_{T,2}$, we set $\{\theta_0, \varphi_0, \sigma_\theta, \kappa\}$'s to $\left\{\frac{\pi}{3}, \frac{2\pi}{3}, \frac{\pi}{10}, 5\right\}$ and $\left\{\frac{\pi}{3}, \frac{\pi}{3}, \frac{\pi}{10}, 5\right\}$, respectively, where σ_θ is the PAS standard deviation of the elevation angle and κ is the concentration parameter of the Von-Mises distribution.

The large-scale path loss is modeled as $f_{\mathrm{path}}(\bar{d}) = \bar{d}^{-n_0}$, where $\bar{d}$ is the path distance and n_0 is the exponent. The tuples $\{\bar{d}, n_0\}$'s are set to $\{100\,\mathrm{m}, 3.5\}$, $\{80\,\mathrm{m}, 2.3\}$, and $\{40\,\mathrm{m}, 2.2\}$ for the direct link, the transmitter to IRS link, and the IRS to receiver link, respectively. Besides, the noise covariance matrix $\mathbf{R_n} = 3.2 \times 10^{-10} \mathbf{I}_4$ W and the number of data streams $d = 2$. Unless specified otherwise, these parameter settings are available for all examples in this section.

A. Joint Design with Perfect CSI

We introduce six benchmark schemes for comparison:

1) No IRS: Design the optimal $\mathbf{F}$ and $\mathbf{G}$ without IRS.

2) Isotropic transmission: Set $\mathbf{F} = \sqrt{\frac{P_T}{d}} \begin{bmatrix} \mathbf{I}_d & \mathbf{0} \end{bmatrix}^T$. Optimize $\mathbf{G}$ according to (5) and $\boldsymbol{\Phi}$ with *Algorithm 1.1*.

3) Beamforming: The special case presented in Section III.D.

4) Random reflection coefficients: Randomly generate $\{\alpha_i\}_{i=1}^M$ with $|\alpha_i| \leq 1, \forall i$. Optimize $\mathbf{F}$ and $\mathbf{G}$ according to (7) and (5).
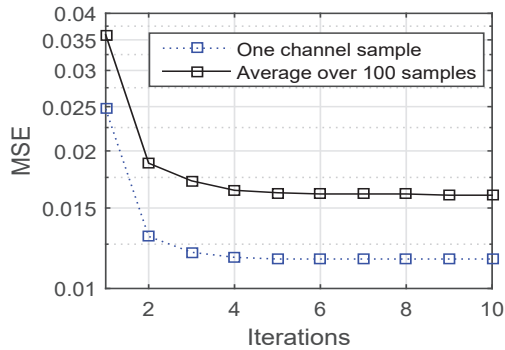
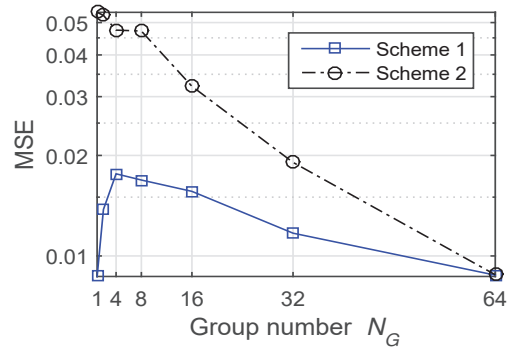Fig. 2: The convergence of the proposed *Algorithm 1*.

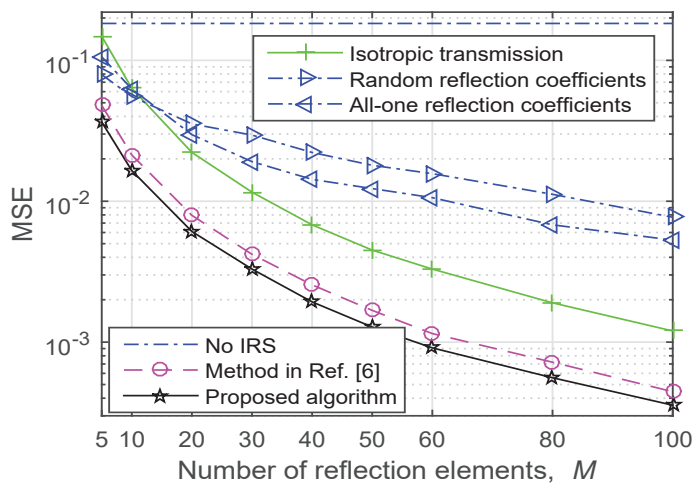Fig. 6 MSE performance for group-based schemes.

Fig. 3: The effect of the element number M on MSE.

5) All-one reflection coefficients: Set $\alpha_i = 1, \forall i$ and only optimize $\mathbf{F}$ and $\mathbf{G}$.

6) Method in Ref. [6]: Obtain the optimal transmission covariance matrix $\mathbf{Q}$ and the co-efficients $\{\alpha_i\}_{i=1}^{M}$ by [6, *Algorithm* 1]. Note that when optimizing $\mathbf{Q}$ with the classic water-filling method, the maximum number of data streams, to which the power can be allocated, is d. Then, solve $\mathbf{F} = \sqrt{\mathbf{Q}}$ and $\mathbf{G}$ by (5).

Fig. 2 shows the convergence behaviour of the proposed *Algorithm* 1, where $M = 10$ and $P_T = 15$ dBmW. The MSE with one channel sample and that averaged over 100 independent channel samples are presented. For both cases, the MSEs decrease monotonically and converge after $4 \sim 6$ iterations.

Fig. 3 shows the effect of the element number M on MSE, with $P_T = 15$ dBmW. Observe that, the isotropic transmission has poor performance at small M. When $M > 20$, it outperforms the benchmark schemes 4 and 5. With moderate or large M, all the schemes with IRS are
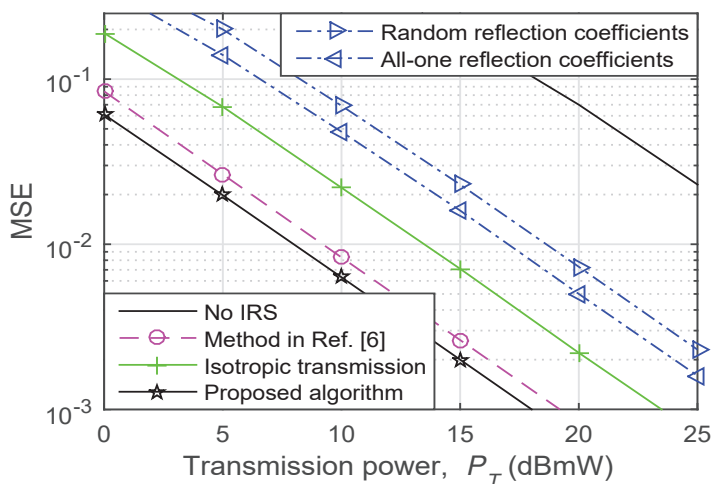
Fig. 4: The effect of the transmission power P_T on MSE.

superior to that without IRS, i.e., the benchmark scheme 1. The performance of the method in [6] is the second only to the proposed algorithm. This is due to the fact that the design objective of the method in [6] is to maximize the capacity, which is different from the objective in this paper. Besides, the MSEs for all the schemes with IRS decrease monotonically with M, which illustrates that large reflection elements are able to bring the performance gain.

Fig. 4 presents the effect of the transmission power P_T on MSE, with $M = 40$. Observe that, all MSEs decreases with P_T. It is clear that increasing P_T leads to larger signal-to-noise ratio (SNR) and better performance. The isotropic transmission outperforms the benchmark schemes 4 and 5, which demonstrates the importance of optimizing the coefficients $\{\alpha_i\}$. Compared with the benchmark scheme 6, the proposed algorithm has about 1.0 dB power gain within $0 \le P_T \le 25$ dBmW. Again, the proposed algorithm has the best performance, followed by the benchmark scheme 6.

Fig. 5 shows the effect of the UPA correlation on MSE, where $M = 40$, $P_T = 15$ dBmW, and the exponential model is used for the modelling of UPA. The correlation coefficient between two IRS elements with co-ordinates (i_1, j_1) and (i_2, j_2) is $(\rho^{\mathrm{cov}})^{\sqrt{(i_1-i_2)^2+(j_1-j_2)^2}}$ with $\rho^{\mathrm{cov}} \in [0, 1]$. Observe that, the proposed algorithm is superior to all benchmark schemes except for the beamforming. This is because the number of data streams for beamforming is 1, less than the predetermined $d = 2$ for all other schemes. The lower MSE of beamforming is achieved at the cost of transmission rate. Besides, the MSE for the proposed algorithm is not affected by the
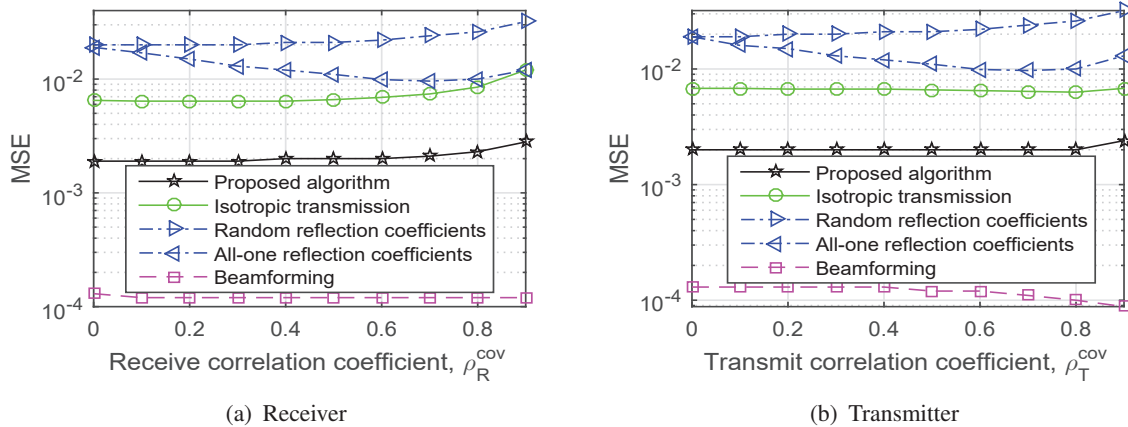
(a) Receiver   (b) Transmitter

Fig. 5: The effect of UPA correlation on MSE.

TABLE I: IRS group parameters

Group number N_G	1	2	4	8	16	32	64
Group size	8×8	4×8	4×4	2×4	2×2	1×2	1×1

transmit or receive correlation within a wide range, e.g. $0 \leq \rho^{\text{cov}} \leq 0.7$, except for a slight increase at large ρ^{cov}. This illustrates that the proposed algorithm can overcome the impact of UPA correlation to some degree.

Fig. 6 depicts the MSE performance of two group-based schemes, where an IRS of size 8×8 is used and partitioned into a few groups whose sizes are given by Table I. Both intergroup and intragroup coefficients are optimized for Scheme 1 while only intergroup coefficients for Scheme 2. The details of them can be found in Section III.D. Observe that, the MSE for Scheme 2 decreases with N_G monotonically. Due to the increase of the optimized variables for $N_G \geq 8$, the MSE for Scheme 1 raises first and then decreases. Compared with Scheme 2, Scheme 1 has smaller variation and exhibits better MSE performance.

B. Robust Design with Channel Uncertainties

This subsection evaluates the performance of the proposed *Algorithm* 2. The channel samples are generated according to (1). We employ the conventional MMSE method [42] to obtain the cascaded channel estimates $\{\widehat{\mathbf{L}}_m\}$. Subsequently, the row covariance matrix of $\Delta\mathbf{L}_m$, $\mathbf{\Theta}_{\text{A,IRS}} = g_1 g_2 \sigma_e^2 \left(\mathbf{I}_{N_R} + \sigma_e^2 \mathbf{\Psi}_{R,2}^{-1}\right)^{-1}$ and the column covariance matrix of $\Delta\mathbf{L}_m$, $\mathbf{\Theta}_{\text{B,IRS}} = \mathbf{\Psi}_{T,1}$.

Fig. 7 shows the convergence behaviour of the proposed *Algorithm* 2, where $M = 50$ and $P_T = 15$ dBmW. Two cases with $\sigma_e^2 = 0.05$ and $\sigma_e^2 = 0.15$ are incorporated; for each case, we

26

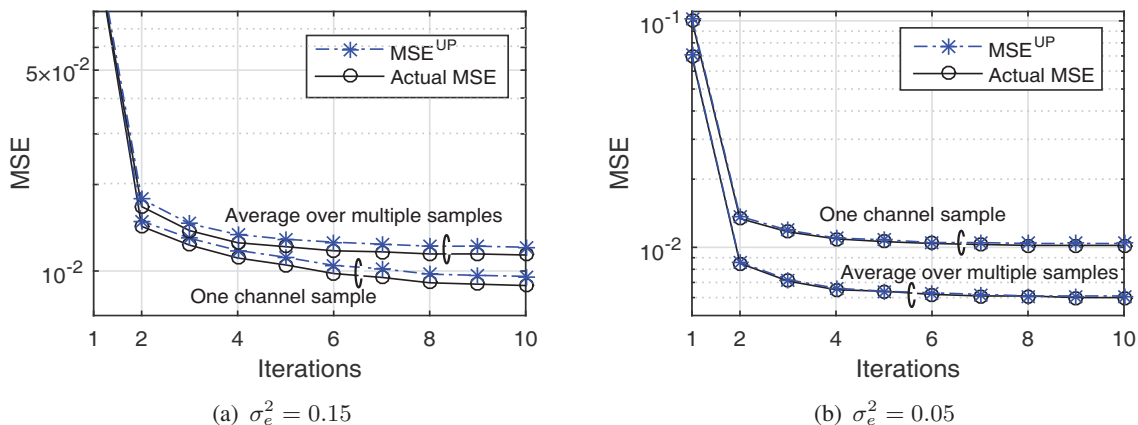(a) $\sigma_e^2 = 0.15$ (b) $\sigma_e^2 = 0.05$

Fig. 7: The convergence of the proposed Algorithm 2.

provide the MSE iterate under a single channel realization as well as that averaged over 100 channel samples. As in Fig. 7a, although we aim at optimizing the MSE upper bound, $\mathrm{MSE}^{\mathrm{UP}}$ in (28), the convergence behaviour of the actual MSE is quite similar to that of $\mathrm{MSE}^{\mathrm{UP}}$. Both MSEs decrease with iterations and converges only after $5 \sim 8$ iterations, except for a certain MSE gap. The MSE gap between $\mathrm{MSE}^{\mathrm{UP}}$ and the actual MSE decreases with decreasing σ_e^2. For the case in which the MSE is averaged over 100 channel samples, the MSE gap for $\sigma_e^2 = 0.15$ is around 5.0×10^{-4}, as compared to 1.2×10^{-4} for $\sigma_e^2 = 0.05$.

Figs. 8 and 9 investigate the impacts of the element number M and transmission power P_T on MSE. Here, the MSE refers to the actual MSE, not the upper bound $\mathrm{MSE}^{\mathrm{UP}}$. Besides, each point in these figures is an average over 100 independent channel realizations. Three designs are included for comparison: the exact design with perfect CSI, the non-robust design (which assumes the channel estimate as perfect), and the proposed robust design against imperfect CSI. In addition, we set $P_T = 15$ dBmW in Fig. 8 and $M = 50$ in Fig. 9. Observe From Fig. 8 that the MSE with the proposed robust design decreases with M but the opposite is found for the non-robust design. This is probably because the non-robust ignores the estimation errors and increasing M brings about more channel uncertainties. Besides, large estimation error σ_e^2 degrades the MSE performance for both the robust and non-robust designs. From Fig. 9, all MSEs decrease with P_T. Given σ_e^2, the MSE of the proposed robust design is always less than that of the non-robust design. The results of the two figures have demonstrated the effectiveness of the proposed robust design.

Fig. 10 compares the BERs of the proposed robust design, the non-robust design, and the

27
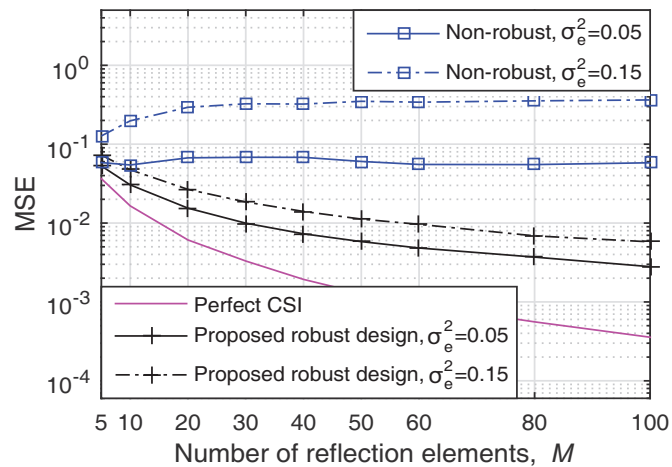
Fig. 8: The effect of the element number M on MSE.
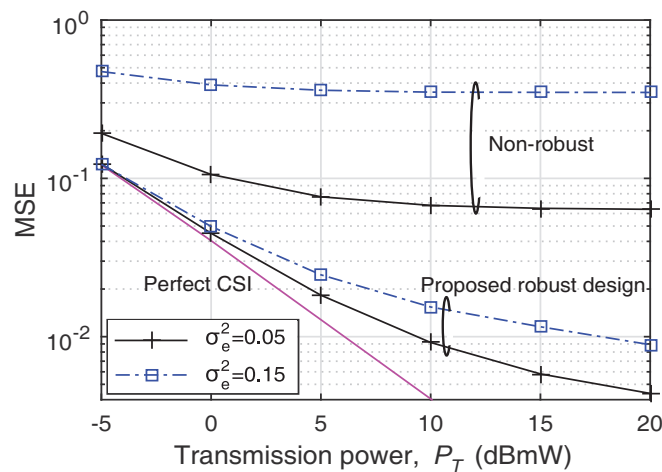
Fig. 9: The effect of the transmission power P_T on MSE.

exact design with perfect CSI, where $M = 50$ and the QPSK modulation is employed. Observe that, for the non-robust design, large estimation error, e.g. $\sigma_e^2 = 0.15$, results in a BER floor of 0.015. For both the robust and non-robust designs, their BER performance improves when σ_e^2 decreases. Given σ_e^2, the robust design is superior to the non-robust one. These results are in line with the MSE performance in Fig. 9.

VI. CONCLUSIONS

In this work, we investigated the joint transceiver and IRS design in IRS-assisted MIMO systems under both perfect and imperfect CSI conditions. The detection MSE was minimized by jointly optimizing the precoder at the transmitter, reflection coefficients at the IRS, and equalizer at the receiver. For the design with perfect CSI, the SPOC algorithm was proposed to
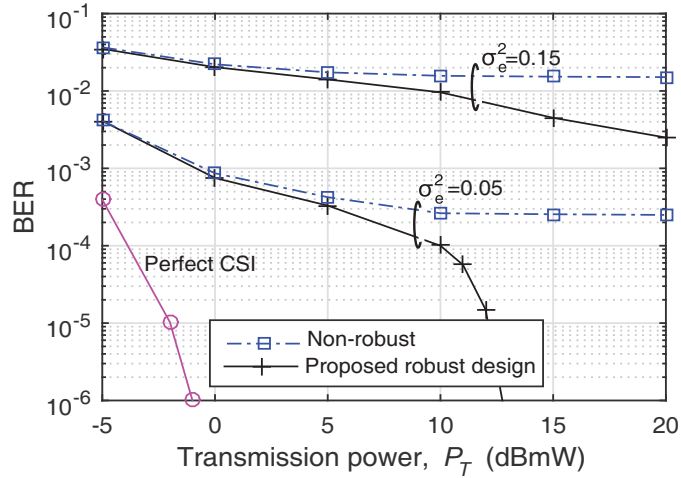
Fig. 10: The BERs of the proposed robust design and a few other algorithms.

solve the optimal IRS reflection coefficients successively. For the robust design with imperfect CSI, the detection MSE was averaged over channel uncertainties and an MSE upper bound was derived and used to make the problem more tractable. Numerical results demonstrated the convergence of the proposed algorithms. The proposed joint design under perfect CSI is superior to all the benchmark schemes with or without the IRS. Compared with the non-robust design, the proposed robust design achieves better performance in terms of both MSE and BER. Besides, the application of IRS is beneficial to improving the system performance even under the imperfect CSI.

Appendix A

Derivation of Eq. (13)

Substituting (11) into (10), we have

$$
\begin{aligned}
q(\rho_m, \phi_m) &= \mathrm{Tr}\left[\mathbf{A}_m^{-\frac{1}{2}}\left(\mathbf{I}_d + \rho_m e^{j\phi_m}\mathbf{U}_m\mathbf{C}_m\mathbf{U}_m^H + \rho_m e^{-j\phi_m}\mathbf{U}_m\mathbf{C}_m^H\mathbf{U}_m^H\right)^{-1}\mathbf{A}_m^{-\frac{1}{2}}\right] \\
&= \mathrm{Tr}\left[\mathbf{A}_m^{-\frac{1}{2}}\mathbf{U}_m\left(\mathbf{I}_d + \rho_m e^{j\phi_m}\mathbf{C}_m + \rho_m e^{-j\phi_m}\mathbf{C}_m^H\right)^{-1}\mathbf{U}_m^H\mathbf{A}_m^{-\frac{1}{2}}\right] \\
&= \mathrm{Tr}\left[\mathbf{U}_m^H\mathbf{A}_m^{-1}\mathbf{U}_m\left(\mathbf{I}_d + \rho_m e^{j\phi_m}\mathbf{C}_m + \rho_m e^{-j\phi_m}\mathbf{C}_m^H\right)^{-1}\right].
\end{aligned}
\tag{31}
$$

With *Lemma 1*, $\left(\mathbf{I}_d + \rho_m e^{j\phi_m}\mathbf{C}_m + \rho_m e^{-j\phi_m}\mathbf{C}_m^H\right)$ has the following form:

$$
\mathbf{I}_d + \rho_m e^{j\phi_m}\mathbf{C}_m + \rho_m e^{-j\phi_m}\mathbf{C}_m^H = \begin{bmatrix} \bar{c}_{11} & \bar{\mathbf{c}}^H \\ \bar{\mathbf{c}} & \mathbf{I}_{d-1} \end{bmatrix},
$$

where $\bar{c}_{11} = 1 + \rho_m e^{j\phi_m} c_{11} + \rho_m e^{-j\phi_m} c_{11}^*$, and $\bar{\mathbf{c}} = \rho_m e^{-j\phi_m} \begin{bmatrix} c_{12} & \cdots & c_{1d} \end{bmatrix}^H \in \mathbb{C}^{(d-1)\times 1}$.

To find $(\mathbf{I}_d + \rho_m e^{j\phi_m} \mathbf{C}_m + \rho_m e^{-j\phi_m} \mathbf{C}_m^H)^{-1}$, we present the inverse of a partitioned matrix. Let $\mathbf{X}$ be partitioned as a 2-by-2 block matrix $\mathbf{X} = \begin{bmatrix} \mathbf{X}_{11} & \mathbf{X}_{12} \\ \mathbf{X}_{21} & \mathbf{X}_{22} \end{bmatrix}$. The inverse of $\mathbf{X}$ is [38, Eq. (0.7.3.1)]

$$\mathbf{X}^{-1} = \begin{bmatrix} \left(\mathbf{X}_{11} - \mathbf{X}_{12}\mathbf{X}_{22}^{-1}\mathbf{X}_{21}\right)^{-1} & \mathbf{X}_{11}^{-1}\mathbf{X}_{12}\left(\mathbf{X}_{21}\mathbf{X}_{11}^{-1}\mathbf{X}_{12} - \mathbf{X}_{22}\right)^{-1} \\ \mathbf{X}_{22}^{-1}\mathbf{X}_{21}\left(\mathbf{X}_{12}\mathbf{X}_{22}^{-1}\mathbf{X}_{21} - \mathbf{X}_{11}\right)^{-1} & \left(\mathbf{X}_{22} - \mathbf{X}_{21}\mathbf{X}_{11}^{-1}\mathbf{X}_{12}\right)^{-1} \end{bmatrix}. \quad (32)$$

With (32), we have

$$(\mathbf{I}_d + \rho_m e^{j\phi_m} \mathbf{C}_m + \rho_m e^{-j\phi_m} \mathbf{C}_m^H)^{-1} = \frac{1}{\bar{c}_{11} - \|\bar{\mathbf{c}}\|_F^2} \begin{bmatrix} 1 & -\bar{\mathbf{c}}^H \\ -\bar{\mathbf{c}} & \left(\bar{c}_{11} - \|\bar{\mathbf{c}}\|^2\right)\mathbf{I}_{d-1} + \bar{\mathbf{c}}\bar{\mathbf{c}}^H \end{bmatrix}. \quad (33)$$

Substitute (33) and (12) into (31), obtaining $q(\rho_m, \phi_m) = \frac{1}{\bar{c}_{11} - \|\bar{\mathbf{c}}\|_F^2}\left[t_{11} - 2\mathrm{Re}\left\{\mathbf{t}_{21}^H\bar{\mathbf{c}}\right\} + \mathrm{Tr}\left(\mathbf{T}_{22}\bar{\mathbf{c}}\bar{\mathbf{c}}^H\right)\right] + \mathrm{Tr}\left(\mathbf{T}_{22}\right)$. It is clear that, $\|\bar{\mathbf{c}}\|_F^2$, $\mathrm{Tr}\left(\mathbf{T}_{22}\bar{\mathbf{c}}\bar{\mathbf{c}}^H\right)$ and $\mathrm{Tr}\left(\mathbf{T}_{22}\right)$ are not related with ϕ_m and they can be treated as constants. Let $c_{11} \triangleq \rho_c e^{j\phi_c}$ and $\bar{\mathbf{c}}^H \mathbf{t}_{21}/e^{j\phi_m} = \rho_m \begin{bmatrix} c_{12} & \cdots & c_{1d} \end{bmatrix} \mathbf{t}_{21} \triangleq \rho_t e^{j\phi_t}$. $q(\rho_m, \phi_m)$ can be finally arranged as

$$q(\rho_m, \phi_m) = \frac{\left[t_{11} + \mathrm{Tr}\left(\mathbf{T}_{22}\bar{\mathbf{c}}\bar{\mathbf{c}}^H\right)\right] - 2\rho_t \cos\left(\phi_m + \phi_t\right)}{\left(1 - \|\bar{\mathbf{c}}\|_F^2\right) + 2\rho_c \cos\left(\phi_m + \phi_c\right)} + \mathrm{Tr}\left(\mathbf{T}_{22}\right).$$

APPENDIX B

PROOF OF *Proposition 1*

Introducing an auxiliary variable $v_m \geq 0$, the Lagrangian associated with $\mathrm{P}_{2\text{-m}}$ is

$$\mathcal{L}\left(\alpha_m, v_m\right) = \mathrm{Tr}\left[\left(\mathbf{A}_m + \alpha_m \mathbf{B}_m + \alpha_m^* \mathbf{B}_m^H\right)^{-1}\right] + v_m\left(|\alpha_m|^2 - 1\right).$$

It is clear that the optimal solution to $\mathrm{P}_{2\text{-m}}$ satisfies the KKT conditions: $\frac{\partial \mathcal{L}(\alpha_m, v_m)}{\partial \alpha_m} = 0$, $v_m\left(|\alpha_m|^2 - 1\right) = 0$, $v_m \geq 0$, and $|\alpha_m| - 1 \leq 0$. When $v_m = 0$, it follows that

$$\frac{\partial \mathcal{L}(\alpha_m, v_m)}{\partial \alpha_m^*} = -\mathrm{Tr}\left\{\left(\mathbf{A}_m + \alpha_m \mathbf{B}_m + \alpha_m^* \mathbf{B}_m^H\right)^{-2}\left[\alpha_m\left(\tilde{\mathbf{r}}_m\tilde{\mathbf{t}}_m^T\right)^H\left(\tilde{\mathbf{r}}_m\tilde{\mathbf{t}}_m^T\right) + \mathbf{B}_m^H\right]\right\} = 0. \quad (34)$$

If α_m satisfies (34) and $|\alpha_m| \leq 1$, it satisfies all KKT conditions and hence, it is a candidate for the optimal solution. Otherwise, v_m can not be 0 and it follows that $|\alpha_m| = 1$.

30

Appendix C

Proof of *Lemma 3*

First, we note that the objectives of $P_{3\text{-}1}$ and $P'_{3\text{-}1}$ are identical. Obviously, if the pair $\{\mathbf{F}, \bar{\mathbf{F}}\}$ is feasible for $P_{3\text{-}1}$, then $\bar{\mathbf{F}}$ is also feasible for $P'_{3\text{-}1}$. It follows that the optimal value of $P_{3\text{-}1}$ is larger than or equal to that of $P'_{3\text{-}1}$.

Conversely, if $\bar{\mathbf{F}}$ is feasible for $P'_{3\text{-}1}$, with $\mathbf{F} \triangleq \sqrt{P_T}\mathbf{D}^{-\frac{1}{2}}\bar{\mathbf{F}}/\sqrt{\mathrm{Tr}\left(\bar{\mathbf{F}}^H\mathbf{D}^{-1}\bar{\mathbf{F}}\right)}$, the pair $\{\mathbf{F}, \bar{\mathbf{F}}\}$ is feasible for $P_{3\text{-}1}$. Therefore, the optimal value of $P_{3\text{-}1}$ is less than or equal to that of $P'_{3\text{-}1}$.

Based on the above analysis, we conclude that $P_{3\text{-}1}$ and $P'_{3\text{-}1}$ are equivalent.

References

[1] Q. Wu and R. Zhang, "Towards smart and reconfigurable environment: Intelligent reflecting surface aided wireless network," *IEEE Communications Magazine*, vol. 58, no. 1, pp. 106–112, 2020.

[2] W. Tang, J. Dai, M. Chen, X. Li, Q. Chen, S. Jin, K.-K. Wong, and T. J. Cui, "Programmable metasurface-based RF chain-free 8PSK wireless transmitter," *Electronics letters*, vol. 55, no. 7, pp. 417–420, 2019.

[3] T. Shafique, H. Tabassum, and E. Hossain, "Optimization of wireless relaying with flexible UAV-borne reflecting surfaces," *IEEE Transactions on Communications*, vol. 69, no. 1, pp. 309–325, 2021.

[4] H. Shen, W. Xu, S. Gong, Z. He, and C. Zhao, "Secrecy rate maximization for intelligent reflecting surface assisted multi-antenna communications," *IEEE Communications Letters*, vol. 23, no. 9, pp. 1488–1492, 2019.

[5] Z. Chu, W. Hao, P. Xiao, D. Mi, Z. Liu, M. Khalily, J. R. Kelly, and A. P. Feresidis, "Secrecy rate optimization for intelligent reflecting surface assisted MIMO system," *IEEE Transactions on Information Forensics and Security*, vol. 16, pp. 1655–1669, 2021.

[6] S. Zhang and R. Zhang, "Capacity characterization for intelligent reflecting surface aided MIMO communication," *IEEE Journal on Selected Areas in Communications*, vol. 38, no. 8, pp. 1823–1838, 2020.

[7] J. Zhang, J. Liu, S. Ma, C.-K. Wen, and S. Jin, "Large system achievable rate analysis of RIS-assisted MIMO wireless communication with statistical CSIT," *IEEE Transactions on Wireless Communications*, vol. 20, no. 9, pp. 5572–5585, 2021.

[8] B. Ning, Z. Chen, W. Chen, and J. Fang, "Beamforming optimization for intelligent reflecting surface assisted MIMO: A sum-path-gain maximization approach," *IEEE Wireless Communications Letters*, vol. 9, no. 7, pp. 1105–1109, 2020.

[9] K. Zhi, C. Pan, H. Ren, and K. Wang, "Statistical CSI-based design for reconfigurable intelligent surface-aided massive MIMO systems with direct links," *IEEE Wireless Communications Letters*, vol. 10, no. 5, pp. 1128–1132, 2021.

[10] A. Abrardo, D. Dardari, and M. Di Renzo, "Intelligent reflecting surfaces: Sum-rate optimization based on statistical position information," *IEEE Transactions on Communications*, vol. 69, no. 10, pp. 7121–7136, 2021.

[11] C. Pan, H. Ren, K. Wang, W. Xu, M. Elkashlan, A. Nallanathan, and L. Hanzo, "Multicell MIMO communications relying on intelligent reflecting surfaces," *IEEE Transactions on Wireless Communications*, vol. 19, no. 8, pp. 5218–5233, 2020.

[12] J. Ye, S. Guo, and M.-S. Alouini, "Joint reflecting and precoding designs for SER minimization in reconfigurable intelligent surfaces assisted MIMO systems," *IEEE Transactions on Wireless Communications*, vol. 19, no. 8, pp. 5561–5574, 2020.

31

[13] W. Mei and R. Zhang, "Multi-beam multi-hop routing for intelligent reflecting surfaces aided massive MIMO," *IEEE Transactions on Wireless Communications*, pp. 1–1, 2021.

[14] J. Li, L. Zhang, K. Xue, Y. Fang, and Q. Sun, "Secure transmission by leveraging multiple intelligent reflecting surfaces in miso systems," *IEEE Transactions on Mobile Computing*, pp. 1–1, 2021.

[15] Y. Ma, R. Liu, M. Li, and Q. Liu, "Passive information transmission in intelligent reflecting surface aided miso systems," *IEEE Communications Letters*, vol. 24, no. 12, pp. 2951–2955, 2020.

[16] Q. Wu and R. Zhang, "Beamforming optimization for wireless network aided by intelligent reflecting surface with discrete phase shifts," *IEEE Transactions on Communications*, vol. 68, no. 3, pp. 1838–1851, 2020.

[17] W. Shi, J. Li, G. Xia, Y. Wang, X. Zhou, Y. Zhang, and F. Shu, "Secure multigroup multicast communication systems via intelligent reflecting surface," *China Communications*, vol. 18, no. 3, pp. 39–51, 2021.

[18] G. Zhou, C. Pan, H. Ren, K. Wang, and A. Nallanathan, "Intelligent reflecting surface aided multigroup multicast MISO communication systems," *IEEE Transactions on Signal Processing*, vol. 68, pp. 3236–3251, 2020.

[19] W. Ni, Y. Liu, and H. Tian, "Intelligent reflecting surfaces enhanced federated learning," in *Proc. IEEE Global Communications Conference (GLOBECOM) Workshops*, 2020, pp. 1–6.

[20] S. Gong, C. Xing, X. Zhao, S. Ma, and J. An, "Unified IRS-aided MIMO transceiver designs via majorization theory," *IEEE Transactions on Signal Processing*, vol. 69, pp. 3016–3032, 2021.

[21] S. Hong, C. Pan, H. Ren, K. Wang, A. Nallanathan, and H. Li, "Robust transmission design for intelligent reflecting surface aided secure communications," in *Proc. IEEE Global Communications Conference (GLOBECOM)*, 2020, pp. 1–6.

[22] G. Zhou, C. Pan, H. Ren, K. Wang, M. D. Renzo, and A. Nallanathan, "Robust beamforming design for intelligent reflecting surface aided MISO communication systems," *IEEE Wireless Communications Letters*, vol. 9, no. 10, pp. 1658–1662, 2020.

[23] G. Zhou, C. Pan, H. Ren, K. Wang, and A. Nallanathan, "A framework of robust transmission design for IRS-aided MISO communications with imperfect cascaded channels," *IEEE Transactions on Signal Processing*, vol. 68, pp. 5092–5106, 2020.

[24] X. Hu, C. Zhong, M. S. Alouini, and Z. Zhang, "Robust design for IRS-aided communication systems with user location uncertainty," *IEEE Wireless Communications Letters*, vol. 10, no. 1, pp. 63–67, 2021.

[25] Y. Omid, S. M. Shahabi, C. Pan, Y. Deng, and A. Nallanathan, "Low-complexity robust beamforming design for IRS-aided MISO systems with imperfect channels," *IEEE Communications Letters*, vol. 25, no. 5, pp. 1697–1701, 2021.

[26] Y. Huang, X. Su, D. Wu, J. Jin, Q. Wang, and J. Wang, "Robust transmission design for IRS aided distributed MISO with imperfect cascaded CSIT," in *Proc. IEEE Wireless Communications and Networking Conference (WCNC)*, 2021, pp. 1–7.

[27] J. Zhang, Y. Zhang, C. Zhong, and Z. Zhang, "Robust design for intelligent reflecting surfaces assisted MISO systems," *IEEE Communications Letters*, vol. 24, no. 10, pp. 2353–2357, 2020.

[28] X. Yu, D. Xu, D. W. K. Ng, and R. Schober, "IRS-assisted green communication systems: Provable convergence and robust optimization," *IEEE Transactions on Communications*, 2021, doi: 10.1109/TCOMM.2021.3087794.

[29] Q. Wang, F. Zhou, R. Q. Hu, and Y. Qian, "Energy efficient robust beamforming and cooperative jamming design for IRS-assisted MISO networks," *IEEE Transactions on Wireless Communications*, vol. 20, no. 4, pp. 2592–2607, 2021.

[30] T. David and P. Viswanath, *Fundamentals of Wireless Communication*. Cambridge University Press, 2004.

[31] C. Oestges and B. Clerckx, *MIMO Wireless Communications: From Real World Propagation to Space-Time Code Design*. Elsevier, 2007.

[32] T. Van Chien, H. Q. Ngo, S. Chatzinotas, and B. Ottersten, "Reconfigurable intelligent surface-assisted massive MIMO: Favorable propagation, channel hardening, and rank deficiency," available at: https://arxiv.org/pdf/2107.03434.pdf.

32

[33] A. Forenza, D. J. Love, and R. W. Heath, "Simplified spatial correlation models for clustered MIMO channels with different array configurations," *IEEE Transactions on Vehicular Technology*, vol. 56, no. 4, pp. 1924–1934, 2007.

[34] D.-S. Shiu, G. J. Foschini, M. J. Gans, and J. M. Kahn, "Fading correlation and its effect on the capacity of multielement antenna systems," *IEEE Transactions on Communications*, vol. 48, no. 3, pp. 502–513, 2000.

[35] H. Lim, Y. Jang, and D. Yoon, "Bounds for eigenvalues of spatial correlation matrices with the exponential model in mimo systems," *IEEE Transactions on Wireless Communications*, vol. 16, no. 2, pp. 1196–1204, 2017.

[36] S. Loyka and J. Mosig, "Channel capacity of n-antenna BLAST architecture," *Electronics Letters*, vol. 36, no. 7, pp. 660–661, 2000.

[37] D. Palomar, J. Cioffi, and M. Lagunas, "Joint Tx-Rx beamforming design for multicarrier MIMO channels: a unified framework for convex optimization," *IEEE Transactions on Signal Processing*, vol. 51, no. 9, pp. 2381–2401, 2003.

[38] R. A. Horn and C. R. Johnson, *Matrix Analysis, 2nd Edition*.   Cambridge University Press, 2012.

[39] M. V. Solodov, "On the convergence of constrained parallel variable distribution algorithms," *SIAM Journal on Optimization*, vol. 8, no. 1, pp. 187–196, 1998.

[40] G. Yan and H. Fan, "A Newton-like algorithm for complex variables with applications in blind equalization," *IEEE Transactions on Signal Processing*, vol. 48, no. 2, pp. 553–556, 2000.

[41] M. Najafi, V. Jamali, R. Schober, and H. V. Poor, "Physics-based modeling and scalable optimization of large intelligent reflecting surfaces," *IEEE Transactions on Communications*, vol. 69, no. 4, pp. 2673–2691, 2021.

[42] M. Ding and S. D. Blostein, "MIMO minimum total MSE transceiver design with imperfect CSI at both ends," *IEEE Transactions on Signal Processing*, vol. 57, no. 3, pp. 1141–1150, 2009.

[43] L. Sanguinetti, A. A. D'Amico, and Y. Rong, "A tutorial on the optimization of amplify-and-forward MIMO relay systems," *IEEE Journal on Selected Areas in Communications*, vol. 30, no. 8, pp. 1331–1346, 2012.

[44] V. P. Singh and A. K. Chaturvedi, "Statistically robust transceiver design algorithms for relay aided multiple-input multiple-output interference systems," *IET Signal Processing*, vol. 12, no. 1, pp. 51–63, 2018.

[45] S. Gong, X. Lu, D. T. Hoang, D. Niyato, L. Shu, D. I. Kim, and Y.-C. Liang, "Toward smart wireless communications via intelligent reflecting surfaces: A contemporary survey," *IEEE Communications Surveys Tutorials*, vol. 22, no. 4, pp. 2283–2314, 2020.

[46] D. Mishra and H. Johansson, "Channel estimation and low-complexity beamforming design for passive intelligent surface assisted MISO wireless energy transfer," in *Proc. IEEE ICASSP*, 2019, pp. 4659–4663.

[47] Y. Yang, B. Zheng, S. Zhang, and R. Zhang, "Intelligent reflecting surface meets OFDM: Protocol design and rate maximization," *IEEE Transactions on Communications*, vol. 68, no. 7, pp. 4522–4535, 2020.

[48] T. Van Chien, H. Q. Ngo, S. Chatzinotas, M. Di Renzo, and B. Ottersten, "Reconfigurable intelligent surface-assisted cell-free massive MIMO systems over spatially-correlated channels," available at https://arxiv.org/pdf/2104.08648.pdf.

[49] Q. Zhang, C. He, and L. Jiang, "Per-stream MSE based linear transceiver design for MIMO interference channels with CSI error," *IEEE Transactions on Communications*, vol. 63, no. 5, pp. 1676–1689, 2015.

[50] A. Chatterjee, S. Chatterjee, and S. S. Das, "Evaluation of spatial correlation and its effect on channel capacity of uniform planar antenna array," in *Proc. National Conference on Communications (NCC)*, 2017, pp. 1–6.